Received: 4 December 2018 | Revised: 11 July 2019 | Accepted: 19 September 2019

DOI: 10.1002/joc.6327

RESEARCH ARTICLE

International Journal of Climatology RMetS

Climate futures for Western Nepal based on regional climate models in the CORDEX-SA

Sanita Dhaubanjar | **Vishnu Prasad Pandey** | **Luna Bharati**

International Water Management Institute (IWMI), Kathmandu, Nepal

Correspondence
Sanita Dhaubanjar, International Water Management Institute (IWMI), Kathmandu, Nepal.
Email: sdhauban@gmail.com

Funding information
Asian Development Bank; Nordic Development Fund; Climate Investment Fund; United States Agency for International Development

Abstract

With the objective to provide a basis for regional climate models (RCMs) selection and ensemble generation for climate impact assessments, we perform the first ever analysis of climate projections for Western Nepal from 19 RCMs in the Coordinated Regional Downscaling Experiment for South Asia (CORDEX-SA). Using the climate futures (CF) framework, projected changes in annual total precipitation and average minimum/maximum temperature from the RCMs are classified into 18 CF matrices for two representative concentration pathways (RCPs: 4.5/8.5), three future time frames (2021–2045/2046–2070/2071–2095), three geographic regions (mountains/hills/plains) and three representative CF (low-risk/consensus/high-risk). Ten plausible CF scenario ensembles were identified to assess future water availability in Karnali basin, the headwaters of the Ganges. Comparison of projections for the three regions with literature shows that spatial disaggregation possible using RCMs is important, as local values are often higher with higher variability than values for South Asia. Characterization of future climate using raw and bias-corrected data shows that RCM projections vary most between mountain and Tarai plains with increasing divergence for higher future and RCPs. Warmer temperatures, prolonged monsoon and sporadic rain events even in drier months are likely across all regions. Highest fluctuations in precipitation are projected for the hills and plains while highest changes in temperature are projected for the mountains. Trends in change in annual average discharge for the scenarios vary across the basin with both precipitation and temperature change influencing the hydrological cycle. CF matrices provide an accessible and simplified basis to systematically generate application-specific plausible climate scenario ensembles from all available RCMs for a rigorous impact assessment.

KEYWORDS

climate model selection, climate projection, CORDEX South Asia, future water resources, Karnali, regional climate model, Western Nepal

1 | INTRODUCTION

Regional climate models (RCMs) are arguably better suited for climate change impact assessments in the heterogeneous and steep terrains of Nepal than global climate models (GCMs; Kundzewicz and Stakhiv, 2010; Flato *et al.*, 2013). The Intergovernmental Panel on Climate Change (IPCC) recognizes that similar to GCMs, RCMs have inherent

limitations and are a work in progress (Stocker *et al*., 2013; Rummukainen *et al*., 2015). Nonetheless, the IPCC reports with *high confidence* that RCMs "add value to the simulation of spatial climate detail in regions with highly variable topography and for mesoscale phenomena such as orographic effect, convection etc." (Pg 815 in Flato *et al*., 2013). Though Coordinated Regional Downscaling Experiment for South Asia (CORDEX-SA) represents the state-of-the-arts in RCMs for South Asia (Giorgi and Gutowski, 2016), evaluation and application of CORDEX-SA over Nepal, specifically at the basin scale, is still lacking. We present the first study to use 19 CORDEX-SA RCMs to generate climate futures (CF) ensembles for water resources assessment in Western Nepal, namely the Karnali basin, with the underlying objective to provide a basis for RCM selection to generate application-specific ensemble projections to suit the specific goals of a climate impact assessment.

Given the abundance of water, steep mountains in the north, rich forests in the mid hills and fertile plains in the south, many plans for developing large hydropower, irrigation and inter-basin water transfer projects exist in Western Nepal (IWMI, 2018a). Nearly 43% of the country's untapped hydropower potential comes from Karnali (Sharma and Awal, 2013). Alongside, Bheri-Babai inter-basin water transfer and the Rani-Jamara Kuleriya irrigation projects are envisioned for mechanization of agriculture. The Digo Jal Bikas (DJB) project is analysing the trade-offs offered by these water resource development visions for Western Nepal to identify pathways and policies that balance sustainable growth, social justice and resilient ecosystems (IWMI, 2018b). Assessment of climate impacts on water resources is indispensable for such long-term planning given that Western Nepal is considered one of the most vulnerable regions within Nepal to climate change (Siddiqui et al., 2012). Western Nepal is also important for the larger Hindu-Kush Himalayas (HKH) as it is the headwaters of the transboundary Ganges river basin. Changes in water availability in Western Nepal will affect flow available downstream in India.

Limited studies address the changing climate in Western Nepal (Shrestha *et al*., 2015; Khatiwada *et al*., 2016) and its impact on water resources (Shiwakoti, 2017; Pandey *et al*., 2019). Fewer studies use RCM ensembles (Karmacharya *et al*., 2007; Devkota *et al*., 2015; Pandey *et al*., 2019). Evaluations of CORDEX-SA RCM performance over the greater South Asian sub-continent and the HKH show that biases exist but RCM performances are promising. Ghimire *et al*. (2015) considering 11 CORDEX-SA RCMs, Sanjay *et al*. (2017a) considering 10 RCMs, Sanjay *et al*. (2017b) considering five RCMs and Mukherjee *et al*. (2017) considering five RCMs show that most RCMs capture spatiotemporal pattern of South Asian precipitation, though skill in reproducing absolute observed values is variable. Nengker *et al*. (2017) and Choudhary and Dimri (2018) considering five different RCMs find similar trends for temperature. Generally, the ensemble outperforms individual RCMs in hindcasting (Ghimire *et al*., 2015; Nengker *et al*., 2017). However, studies highlight that biases in individual CORDEX-SA RCMs vary spatially (geographically and attitudinally) and temporally for both temperature and precipitation for both past (Ghimire *et al*., 2015; Nengker *et al*., 2017) and future climate (Choudhary and Dimri, 2018). Evaluation and correction of spatiotemporal biases is imperative for impact assessment studies, especially those focusing on hydrological application at finer scales, (Wilby, 2010). Quantile-mapping has emerged as promising for correcting RCM and GCM biases in Nepal (Lutz *et al*., 2016; Pandey *et al*., 2019) and abroad (Teutschbein and Seibert, 2012; Themeßl *et al*., 2012; Lafon *et al*., 2013).

Known CORDEX-SA biases also highlight the need for spatial disaggregation in RCM evaluation and application. Furthermore, aggregation to regional scales as done by aforementioned studies may lead to cancellation of spatial variation, especially for climate extremes. Lutz *et al*. (2016) suggest evaluation at scale finer than the South Asian basins done in their study to prevent dilution of local climate signals. Spatial disaggregation is particularly important for Nepal, because it lies in the central part of the HKH characterized by a complex climate regime dependent on the Indian summer monsoon and the winter westerly disturbances (Bookhagen and Burbank, 2010; Palazzi *et al*., 2013). Sanjay *et al*. (2017a, 2017b) find that past performance of CORDEX-SA RCMs is divergent for central HKH. Microclimates occur due to the steep elevations and heterogeneous landscapes in close proximity to the ocean. The past and future trends for precipitation (b; Karmacharya *et al*., 2007; Mcsweeney *et al*., 2010a) and streamflow (Gautam and Acharya, 2012) vary across the east–west and north–south of Nepal.

Large multi-model ensembles are necessary to provide robust characterization of known RCM biases and incorporation of projection uncertainties into climate impact assessments (Wilby, 2010; Sanjay *et al*., 2017b). But past assessments in Nepal are largely based on GCMs (Immerzeel *et al*., 2012; Bharati *et al*., 2014; Shrestha *et al*., 2014; Mishra *et al*., 2018), using at most five models with limited justification for model selection. Such practices consider few deterministic future projections and ignore uncertainties and their dependence on the model selection criteria itself. While the climate modelling community increasingly promotes the use of multi-model ensembles and probabilistic projections for impact assessments (Knutti *et al*., 2010; Stocker *et al*., 2013), real-life application of such datasets is

seldom done by practitioners (Clarke *et al*., 2011; Whetton *et al*., 2012) and hydrologists (Wilby, 2010). Additional burden is levied by having four representative concentration pathways (RCPs) defined as global future scenarios considering anthropogenic changes (van Vuuren *et al*., 2011). Handling multi-model and multi-scenario probabilistic datasets require time, computation resources and technical skills in RCM/GCM data processing and bias correction. Given large uncertainties in observation datasets and models themselves, it is challenging for practitioners in the global south to justify spending their limited resources on the tedious task of generating robust climate projections.

RCM selection methods can help narrow down the ever-increasing pool of models (Whetton *et al*., 2012; Weaver *et al*., 2013; Lutz *et al*., 2016). Aforementioned RCM evaluation studies in South Asia use different models and ensembles and assess different variables–providing limited basis for cross-comparisons. Lutz *et al*. (2016) combine the envelope approach and the past performance approach to identify four representative models out of 94/69 GCMs for RCP 4.5/8.5 for impact assessment in major basins in the HKH. McSweeney *et al*. (2012) reverse the sequence to select GCMs for Vietnam. While Lutz *et al*. (2016) and McSweeney *et al*., (2012)'s approaches are thorough, considering both range of available projections and model skills, their replication to RCMs and finer spatial scale would require significant work. For instance, Bajracharya *et al*. (2018) skip re-application of the method and directly use the four models chosen by Lutz *et al*. (2016) for the entire Indus, Ganges and Brahmaputra basins for their future water resources assessment in Kaligandaki, a small sub-basin of the Ganges. Few existing web-based tools like the KNMI Climate Explorer (https://climexp.knmi.nl/plot atlas form. py) and the World Bank Climate Change Knowledge Portal (CCKP-http://sdwebx.worldbank.org/climateportal/) focus only on comparison of GCMs. CCKP, targeted towards practitioners, is well designed and user-friendly but provides limited help allowing for comparison of only one parameter from two datasets. KNMI suiting technical audience is promising but has a steep learning curve requiring substantial online data processing. Both provide limited support for sub-national analyses.

The Australian Representative Climate Future framework (CSIRO and BOM, 2015, 2018), is a simpler model selection tool catering to the needs of practitioners with limited knowledge and resources, typical in the global south. It allows scientists to provide a snapshot of model projections and associated uncertainties to decision-makers by classifying all projections in a visual matrix (Clarke *et al*., 2011; Whetton *et al*., 2012). Users can then select relevant climate models by focusing on climate risks important to their impact assessment, considering the entire range of projections. As Whetton *et al*. (2012) highlight, the strength of CF framework lies in its scalability and flexibility for generating application-specific climate projections. The framework can be applied across disciplines and spatiotemporal scales, comprising multiple climate parameters, and be updated as new models emerge.

A robust climate impact assessment can only be conducted with robust projections generated through analysis of multiple climate models. The spatial detail captured by RCMs provides a stronger basis than GCMs to generate climate projections at finer scales suitable for local studies in heterogeneous terrains such as in the HKH. But the application of RCMs and the use of multi-model ensembles have been limited, especially in smaller basins in the global south that are often hotspots vulnerable to climate change. To this end, we explore three key matters for the first time for Western Nepal—the usefulness of CF matrices to generate application-specific ensemble climate projections tailored to the needs of a climate impact assessment; the performance of RCMs compared to historical observations at stations in three geographic areas; and the need for spatial disaggregation in climate impact assessment studies. We provide a simple basis for RCM selection and ensemble generation in the form of the first ever CF matrices for Western Nepal. Considering the case of Karnali water resources assessment for long-term water resources planning, we customize the Australian framework to generate spatially disaggregated annual CF matrices synthesizing precipitation and temperature projections extracted from 19 CORDEX-SA RCMs applied to this region for the first time. Using the CF matrices for mountain, hill and Terai regions, we generate climate future ensembles by selectively combining the 19 RCMs, characterize future climate change at annual and seasonal scale and assess the future annual water availability in Karnali for long-term water resource development. In due process, we evaluate and correct RCM biases against station data for Nepal. The spatial disaggregation and station-based bias correction are particularly significant, as past studies have not evaluated climate change at such fine scales. The strength and limitations of the RCM-based annual CF matrices as a decision support tool to generate application-specific climate projections is explored.

2 | MATERIALS AND METHODS

2.1 | Study area

Western Nepal (Figure 1), comprising of the Karnali basin and parts of the Mahakali basin, is one of the most remote and naturally pristine regions of Nepal. The south-to-north elevation ranges from 142 m to 8,143 m (Jarvis *et al*., 2008). With 21 dominant soil types in Karnali and over 18 in

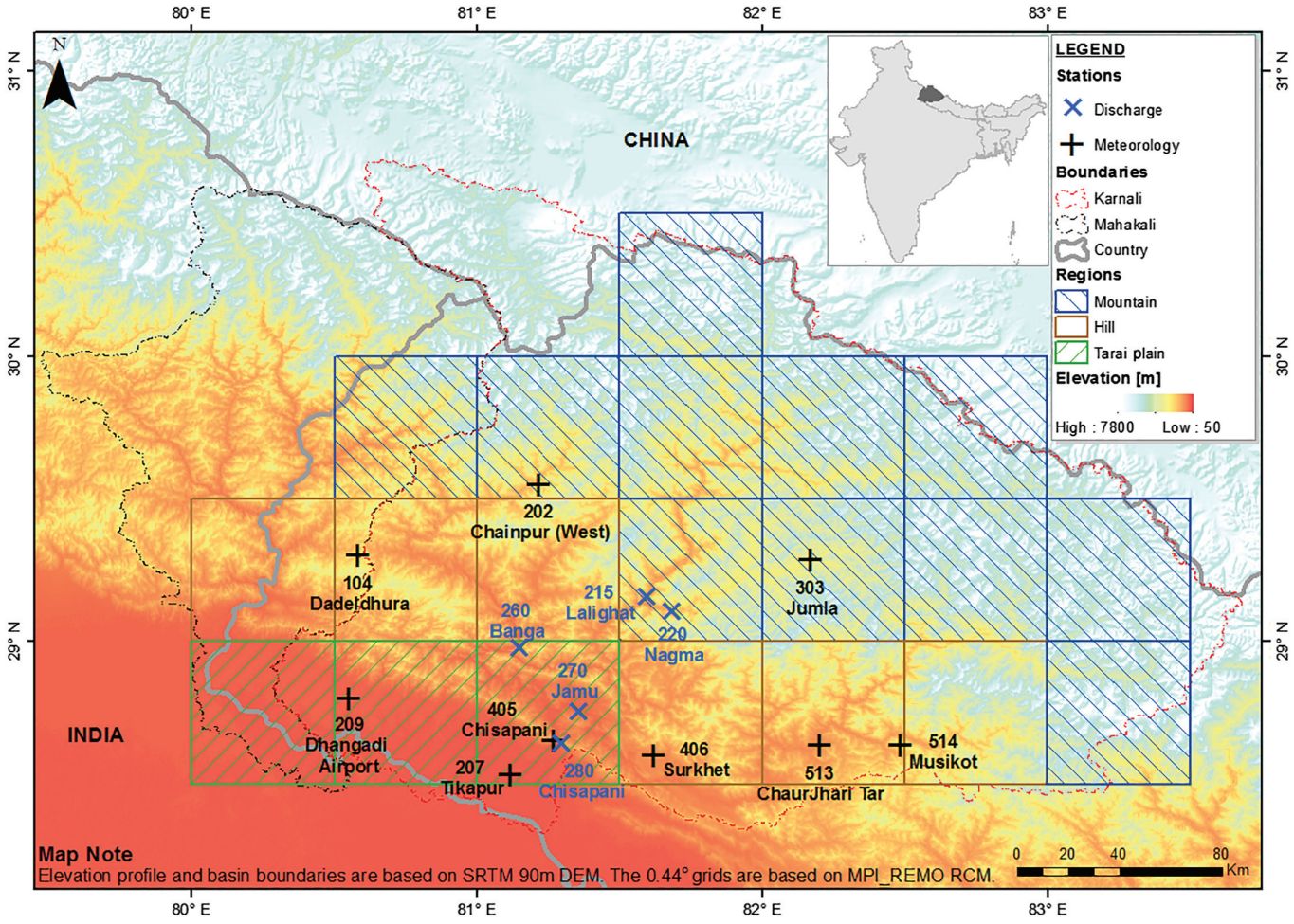

FIGURE 1 Elevation profile and geographic regions of Western Nepal overlaid with the REMO2009 RCM grids whose centres lie within the boundaries of Western Nepal and nine meteorological stations inputs and five discharge stations used for climate change impact assessment study in Karnali [Colour figure can be viewed at wileyonlinelibrary.com]

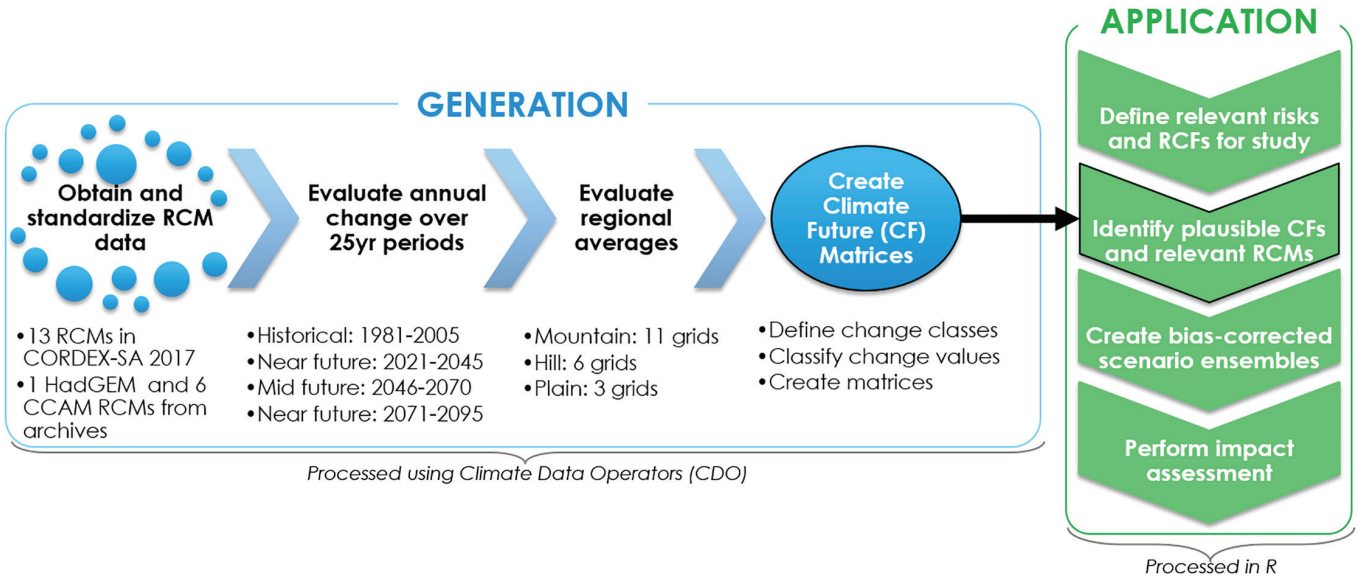

FIGURE 2 Methodology for generation and application of climate futures matrices using the Australian framework (Clarke *et al*., 2011) [Colour figure can be viewed at wileyonlinelibrary.com]

TABLE 1 Description of the 19 CORDEX-SA RCMs in this study. All RCMs have 0.44° spatial resolution. Hits indicate number of times the model was selected for the final climate scenarios

	Short name [GCM_RCM]	Driving GCM	CORDEX-SA RCM description	RCM modelling Centre	Timeframe	Coordinate system	Hits
1.	ACCESS_CCAM	ACCESS1.0	CSIRO-CCAM-1391 M: Conformal cubical atmospheric model (McGregor and Dix, 2001)	Commonwealth scientific and industrial research organization (CSIRO), marine and atmospheric research, Melbourne, Australia	Hist: 1970–2005 RCP4.5/8.5:2006–2099	Regular	15
2.	CNRM_CCAM	CNRM-CM5			Hist: 1970–2005 RCP4.5/8.5:2006–2099	Regular	10
3.	GFDL_CCAM	GFDL-CM3			Hist: 1970–2005 RCP4.5:2006–2070 RCP8.5:2006–2099	Regular	6
4.	MPI_CCAM	MPI-ESM-LR			Hist: 1970–2005 RCP4.5/8.5:2006–2099	Regular	17
5.	NorESM_CCAM	NorESM-M			Hist: 1970–2005 RCP4.5:2006–2099 RCP8.5: None	Regular	7
6.	HadGEM_RA	HadGEM2-AO	HadGEM3-RA: HadGEM3 regional atmospheric model (Moufouma-Okia and Jones, 2014)	Met Office Hadley Centre (MOHC), UK	Hist: 1970–2005 RCP4.5/8.5:2006–2,100	Curvilinear rotated_Latitude _longitude	10
7.	CNRM_RCA4	CNRM-CM5	SMHI-RCA4: Rossby Centre regional atmospheric model version 4 (Samuelsson *et al*., 2011)	Rossby Centre, Swedish Meteorological and Hydrological Institute (SMHI), Sweden	Hist: 1951–2005 RCP: 2006–2,100	Rotated pole	13
8.	ICHEC_RCA4	ICHEC-EC-EARTH			Hist: 1970–2005 RCP: 2006–2,100	Rotated_latitude _Longitude	13
9.	IPSLMR_RCA4	IPSL-CM5A-MR			Hist: 1951–2005 RCP: 2006–2,100	Rotated_pole	2
10.	MIROC5_RCA4	MIROC-MIROC5			Hist: 1951–2005 RCP: 2006–2,100	Rotated_pole	9
11.	MPI_RCA4	MPI-ESM-LR			Hist: 1951–2005 RCP: 2006–2,100	Rotated_pole	10
12.	NOAA_RCA4	NOAA-GFDL -GFDL-ESM2M			Hist: 1951–2005 RCP: 2006–2,100	Rotated_pole	14
13.	MPI_REMO	MPI-ESM-LR	MPI-CSC-REMO2009: MPI regional model 2009 (Teichmann *et al*., 2013)	Climate service Centre (CSC), Germany	Hist: 1970–2005 RCP: 2006–2,100	Regular	8
14.	CanESM2_RegCM4	CCCma-CanESM2	IITM-RegCM4:	Centre for Climate Change Research	Hist: 1951–2005 RCP4.5/8.5:2006–2099	Rotated_mercator	13

(Continues)

TABLE 1 (Continued)

	Short name [GCM_RCM]	Driving GCM	CORDEX-SA RCM description	RCM modelling Centre	Timeframe	Coordinate system	Hits
15.	CNRM_RegCM4	CNRM-CM5	The Abdus Salam International Centre for Theoretical Physics Regional Climatic Model version 4 (Giorgi *et al.*, 2012)	(CCCR), Indian Institute of Tropical Meteorology (IITM), India	Hist: 1951–2005 RCP4.5:2006–2099 RCP8.5:2006–2085	Rotated_mercator	9
16.	CSIRO_RegCM4	CSIRO-Mk3.6			Hist: 1951–2005 RCP4.5/8.5:2006–2099	Rotated_mercator	9
17.	IPSLLR_RegCM4	IPSL-CM5A-LR			Hist: 1951–2005 RCP4.5/8.5:2006–2099	Rotated_mercator	7
18.	MPIMR_RegCM4	MPI-ESM-MR			Hist: 1951–2005 RCP4.5/8.5:2006–2099	Rotated_mercator	8
19.	NOAA_RegCM4	NOAA-GFDL-GFDL-ESM2M			Hist: 1970–2005 RCP: 2006–2099	Curvilinear rotated_mercator	13

Mahakali, there is spatial heterogeneity in biophysical characteristics and biodiversity. The variation is grouped into three geographic regions by the national Department of Survey: mountain, hill and Tarai plains. Karnali, the largest basin in Nepal, drains an area of 49,889 km^2, 35% of which is covered by forests (ICIMOD, 2012). Mahakali is a transboundary river with 32% (~5,628 km^2) of the basin in Nepal, of which 47% are forests. Agriculture (rainfed and irrigated) covers 15% of Karnali and 28% of the Mahakali within Nepal. Between 1980 and 2015, the discharge at Karnali's most downstream station Chisapani (#280) averaged 43 billion m^3/year. Nearly 1,361 glaciers cover 1,740 km^2 and 907 glacial lakes cover 37.7 km^2 (Ives *et al.*, 2010).

2.2 | Generation of climate futures matrices

Figure 2 shows the workflow adapted from Clarke *et al.* (2011). Using Climate Data Operators (Mueller and Schulzweida 2011), RCMs were standardized; regional spatiotemporal averages evaluated; and projected changes classified into annual CF matrices.

2.2.1 | Standardize RCM projections

The 19 RCMs, described in Table 1, are referenced throughout the manuscript with indicated short names, combining names of driving GCM and downscaling RCM. Thirteen RCMs available in the CORDEX-SA, as of December 2017, were downloaded from: https://esg-dn1.nsc.liu.se/search/esgf-liu/. Additionally, one HadGEM_RA and five CSIRO-CCAM RCMs (greyed in Table 1) dated 2014 downloaded from CORDEX-SA in the past were also considered as newer versions were not available in CORDEX-SA at the time of our study. These latter six RCMs, considered in many studies in South Asia (Mcgregor et al., 2013; Thevakaran et al., 2015; Mukherjee *et al.*, 2017), are included to have a comprehensive set of RCMs suitable for Nepal. Only RCPs 4.5 and 8.5, representing the global scenarios for medium and high levels of greenhouse gas emissions (van Vuuren *et al.*, 2011), were available for all 19 RCMs. Hence RCPs 2.6 and 6.0 could not be considered here.

Daily precipitation and near-surface air temperature (min/max) files from all RCMs were visually inspected. Based on overlap between various RCM grids, meteorological stations and geographic regions, the MPI_REMO grids were chosen. All RCMs were re-mapped to MPI_REMO using nearest neighbour method and cropped to the same extent. Units were converted to mm for precipitation and °C for temperature.

2.2.2 | Evaluate annual changes over 25-year periods

Long-term average annual total precipitation (pr) and min/-max temperatures ($t$min/$t$max) were evaluated at each grid for four 25-year timeframes (one historical baseline and three futures) listed in Table 2. The number of RCMs available for each RCP and timeframe varies between 17 and 19. The Δpr, Δ$t$max and Δ$t$min at each grid is evaluated as:

$$\Delta \mathrm{pr}_{\mathrm{RCM,t,RCP}} = \frac{\mathrm{pr}_{\mathrm{RCM,historical}} - \mathrm{pr}_{\mathrm{RCM,t,RCP}}}{\mathrm{pr}_{\mathrm{RCM,historical}}} \times 100$$

$$\Delta t\mathrm{max}_{\mathrm{RCM,t,RCP}} = t\mathrm{max}_{\mathrm{RCM,historical}} - t\mathrm{max}_{\mathrm{RCM,t,RCP}}$$

$$\Delta t\mathrm{min}_{\mathrm{RCM,t,RCP}} = t\mathrm{min}_{\mathrm{RCM,historical}} - t\mathrm{min}_{\mathrm{RCM,t,RCP}}$$

2.2.3 | Evaluate regional averages

Figure 1 shows the 0.44° MPI_REMO grids classified into the northern mountains, the mid-hills and the southern Tarai plains. Table 3 summarizes the coverage for each region. Based on these region definitions, Δpr/Δ$t$max/Δ$t$min across relevant grids were spatially averaged.

2.2.4 | Create CF matrices

The regional Δpr and Δ$t$max/Δ$t$min are categorized into qualitative classes in Table 4 to create six matrices. These classes were defined subjectively, considering the ranges for Australia, the natural climate variability in Western Nepal and local demarcations of climate risks. As suggested by Clarke *et al*. (2011), the classes were defined independent of current models, to accommodate addition of future model additions. The Δpr classes form the rows and Δ$t$max/min form columns of the CF matrix with 35 cells. Each cell is called a *climate future*, representing a combination of Δpr and Δ$t$max/min classes. According to Δpr/Δ$t$max/Δ$t$min obtained, RCMs are assigned to CF cells.

TABLE 2 Time frames considered and number of RCMs available for the two RCP4.5/8.5

Timeframe	Years	# of RCMs in RCP 4.5	# of RCMs in RCP 8.5
Historical	1981–2005	19	19
Near future (NF)	2021–2045	19	18
Mid future (MF)	2046–2070	19	18
Far future (FF)	2071–2095	18	17

TABLE 3 Coverage of the 0.44° grids for mountain, hill and terai plains region

Region	# of grids	Area (km2)	Average elevation (m)
Mountain	11	29,690.9	3,929.9
Hill	6	16,304.2	1,785.8
Plain	3	8,187.7	421.8

2.3 | Application of CF matrices to Karnali

The four-step process for application of the generated CF matrices (Clarke *et al*., 2011) is described in the following. Developed annual CF matrices is applied to identify RCMs that are relevant to the climate risks being addressed by a given study, prepare bias-corrected daily time series data from these and generate ensemble projections for a climate scenario at a station location.

2.3.1 | Define relevant risks and representative climate futures (RCFs)

Climate risks should be identified subjectively in consultation with stakeholders from a practical perspective considering the application at hand. Considering long-term water infrastructure development in this study, stakeholder interaction workshop revealed low-risk future as one where relatively more water is available compared to historical averages, allowing for higher storage in reservoirs and subsequent distribution, but not significantly more water so as to increase the risk of floods and landslides. Conversely, high-risk scenario was defined as one where there is decline in average water availability. Based on the two risk scenarios defined from stakeholder perspective, we defined corresponding representative future climates (RCFs). Hotter and drier climates will create the high-risk scenario. Wetter and warmer conditions will increase precipitation create the low risk scenario. Three RCF have thus been defined considering the two risks, and a maximum consensus as:

- Low-risk: (Δ$t$max: Slightly Warmer *OR* Warmer) + (Δpr: Wetter *OR* Much Wetter)
- Consensus: CF with maximum number of models in the matrix
- High-risk: (Δ$t$max: Hotter *OR* Much Hotter) + (Δpr: Much Drier *OR* Significantly Drier)

2.3.2 | Identify plausible RCFs and relevant RCMs

For each region, there are 18 climate scenarios considering three RCFs, three future timeframes and two RCPs. For each scenario, the RCFs cells in the relevant CF matrix are inspected. If no RCMs are available in the RCF cell, the climate scenario is ignored as implausible. For plausible RCFs,

TABLE 4 Qualitative classifications of projected changes in precipitation and temperature for Western Nepal

Δ Precipitation classes		Δ Temperature classes	
Description	**Range**	**Description**	**Range**
Significantly Drier	$\Delta pr < -25\%$	Colder	$\Delta t < 0°C$
Much Drier	$-25\% \leq \Delta pr < -15\%$	Slightly Warmer	$0 \leq \Delta t < 0.5\ °C$
Drier	$-15\% \leq \Delta pr < -10\%$	Warmer	$0.5\ °C \leq \Delta t < 2.0\ °C$
Little change	$-10\% \leq \Delta pr < 10\%$	Hotter	$2.0°C \leq \Delta t < 3.5°C$
Wetter	$10\% \leq \Delta pr < 15\%$	Much Hotter	$\Delta t \geq 3.5°C$
Much Wetter	$15\% \leq \Delta pr < 25\%$		
Significantly wetter	$\Delta pr \geq 25\%$		

the relevant RCMs are selected to generate daily projections at desired locations.

2.3.3 | Create bias-corrected scenario ensembles

Nine meteorological stations spread throughout Western Nepal (Figure 1), with relatively good quality data were selected for climate characterization. The stations were classified as mountain, hill and Tarai based on their location. For each plausible climate scenario, the relevant RCMs identified for the corresponding region in previous step were gathered. Daily time series was extracted at the station latitude-longitude from these RCMs. Observed station data were compared with RCM simulation data for the historical timeframe (1981–2005) to establish linear functions for bias correcting RCM historical and future projections using empirical quantile-mapping (Gudmundsson *et al*., 2012; Teutschbein and Seibert, 2012). Bias-corrected RCM time-series were then combined as equally weighted multi-model means to generate a single ensemble projection for each climate scenario. See Supporting Information S2 for station details (latitude, longitude, elevation) and the number of RCMs selected to generate scenarios ensembles.

Satellite-based daily climate data was explored to supplement the data from scarcely spread stations for bias correction. However, satellite data were not used because they are poor at capturing topographic dependencies of rainfall (Ghaju and Alfredsen, 2012; Krakauer *et al*., 2013; Peña-Arancibia *et al*., 2013; Bajracharya *et al*., 2015), require application of correction methods specific to the product and location of application (Müller and Thompson, 2013; Thiemig *et al*., 2013), and higher quality products are only available after the 1990s.

The performance of bias correction was evaluated using: the Nash–Sutcliffe Efficiency coefficient (NSE), the percentage bias (PBIAS) and the coefficient of determination (R^2) at seasonal (winter: DJF, pre-monsoon: MAM, monsoon: JJAS), post-monsoon-ON) and annual scales. NSE and R^2 values close to 1 and PBIAS close to 0 indicate good performance, that is, simulated values are statistically close to the observed.

2.3.4 | Perform impact assessment

A hydrological model of Karnali developed by Pandey *et al*. (2018) in Soil and Water Assessment Tool (SWAT; Arnold *et al*., 2012), was used to evaluate changes in average annual discharge (ΔQ) at five discharge stations (Figure 1) in the basin. The model discretized into 111 sub-basins to capture the spatial heterogeneity was forced with the bias-corrected ensemble projections at the nine stations for all plausible climate scenarios.

3 | RESULTS AND DISCUSSION

3.1 | Spatiotemporal variation in simulated future for Western Nepal

Table 5 reports the ranges for change in long-term average annual total precipitation (Δpr) and maximum/minimum temperature (Δ*t*max/min) extracted from the 19 RCMs for Western Nepal. Alongside, Table 5 also presents changes reported by five different climate change studies for the HKH region considering large GCM and RCM ensembles. This study finds that Δ*t*min and Δ*t*max for Western Nepal for RCP 4.5 range 0.6–5.0°C and 0.6–4.0°C, respectively; while for RCP 8.5, Δ*t*min and Δ*t*max range 0.7–9.7°C and 0.6–8.1°C, respectively. The five studies in literature report the annual mean temperature (Δ*t*mean) values over South Asia and the HKH around 0.2–4.5°C and 0.3–7.2°C for RCP 4.5 and 8.5, respectively. These South Asian Δ*t*mean ranges are comparable to the Δ*t*max/tmin for Western Nepal but underestimate Δ*t*max. Similarly, for entire Western Nepal, annual Δpr ranges from −19.2 to 48.3% for RCP 4.5 and −26.1 to 70.7% for RCP 8.5. In contrast, annual Δpr ranges for South Asia are narrower at −5.7 to 27% and −8.5 to 45% for RCP 4.5 and 8.5 scenarios based on the 42 GCMs

TABLE 5 Comparison of ranges in current study with five studies focusing on South Asia. Current study ranges are min and max of the 19 CORDEX-SA RCMs for the mountain, hill and terai plain across the three futures. For literature, min–max or quantiles are reported from sources specified in the last column

	This study				Literature values				
		Mountain	Hill	Plain		Range	Spatial scale	# of models	Source
RCP 4.5	Δpr (%)	[−12.5–33.8]	[−14.5–42.6]	[−19.2–48.3]	Δpr (%)	Annual: [−3–27] ONDJFM: [−18–28] AMJJAS: [−7–37]	South Asia	42 GCMs	1
						Annual: [−5.7–19.4]	Indus, Ganges, Brahmaputra	94 GCMs	2
						JJAS: [0–25] DJF: [−12–8]	Central HKH	10 GCMs	3
						JJAS: [−2–22] DJF: [−17–18]	Central HKH	13 RCMs	3
						JJAS: [−30–30]	HKH	10 RCMs	5
	Δ*t*max [°C]	[0.7–4.0]	[0.6–3.4]	[0.7–3.4]	Δ*t*mean [°C]	Annual: [0.2–3.5] DJF: [0.1–3.7] JJA: [0.3–3.3]	South Asia	42 GCMs	1
						Annual: [1.7–3.6]	Indus, Ganges, Brahmaputra	94 GCMs	2
	Δ*t*min [°C]	[0.6–5.0]	[0.6–3.6]	[0.7–3.5]		JJAS: [1.75–3.2] DJF: [1.5–4.5]	Central HKH	10 GCMs	3
						JJAS: [1.2–2.7] DJF: [1.5–4]	Central HKH	13 RCMs	3
						Annual: [1.0–4.5]	South Asia	5 RCMs	4
RCP 8.5	Δpr (%)	[−17.4–30.8]	[−19.0–48.6]	[−26.1–70.7]	Δpr (%)	Annual: [−7–45] ONDJFM: [−17–42] AMJJAS: [−9–57]	South Asia	39 GCMs	1
						Annual: [−8.5–37.4]	Indus, Ganges, Brahmaputra	69 GCMs	2
						JJAS: [0–35] DJF: [−20–6]	Central HKH	10 GCMs	3
						JJAS: [2–41] DJF: [−30–5]	Central HKH	13 RCMs	3
						JJAS: [−30–30]	Entire HKH	10 RCMs	5
	Δ*t*max (°C)	[1.0–8.1]	[0.7–6.0]	[0.6–5.9]	Δ*t*mean (°C)	Annual: [0.4–6.0] DJF: [0.3–7.1] JJA: [0.3–5.6]	South Asia	39 GCMs	1
						Annual: [3.6–6.5]	Indus, Ganges, Brahmaputra	69 GCMs	2
	Δ*t*min (°C)	[1.1–9.7]	[0.7–6.1]	[0.8–5.7]		JJAS: [2.2–5.5] DJF: [2.6–6.6]	Central HKH	10 GCMs	3
						JJAS: [1.5–4.9] DJF: [2.5–7.2]	Central HKH	13 RCMs	3

Note: 1. For [2016–2095] relative to [1986–2005], reported min–max in Tables 14.1 and 14.SM.1c in (Christensen *et al*., 2013).

2. For [2071–2,100] relative to [1971–2000], reported ranges in section 4.1.1 in (Lutz *et al*., 2016).

3. For [2036–2095] relative to [1976–2005], whiskers in box plot of Figure 9 in (Sanjay *et al*., 2017a).

4. For [2031–2,100] relative to [1976–2005], min–max of annual time series in Figure 7 in (Sanjay *et al*., 2017b).

5. For [2020–2099] relative to [1970–2005], ranges in colour maps in Figures 3 and 4 in (Choudhary and Dimri, 2018).

considered by Christensen *et al*. (2013) and 94 GCMs by Lutz *et al*. (2016). Values for Western Nepal are closer to seasonal precipitation changes reported by Sanjay *et al*. (2017a) and Choudhary and Dimri (2018) based on 10 RCMs. Naturally, our RCM-based ranges are closer to the literature ranges for RCM ensembles than GCMs. The comparison with literature highlights the dilution of climate signal in spatiotemporal aggregation. Local changes can differ from regional and continental changes, especially for precipitation. RCMs should be considered in local studies to resolve finer microclimates within Nepal.

Figure 3 presents the regional changes projected by the 19 RCMs under the two RCPs. The scatter plots show mountain in blue, hill in orange and plains in green; symbols indicate the three future time frames (near: x, mid: + and far: o). RCP 8.5 plot shows higher spatiotemporal spread than RCP 4.5. Scattered points for plains and hills are close to each other while those for the mountain are dispersed. The regions show greater variability in projections as well as diverge progressively from near to far future. Generally, the scattering is wider along the y-axis (Δpr) rather than x-axis (Δ*t*max/min) indicating greater uncertainty in precipitation.

Regional Δ*t*min and Δ*t*max are always positive but the values differ in magnitude and skewness across the regions. In the mountain, Δ*t*min and Δ*t*max points are higher and spread wider along the vertical axis compared to hills and plains, with Δ*t*min varying by 0.6–5.0°C and Δ*t*max by 0.7–4.0°C for RCP 4.5; for RCP 8.5 Δ*t*min ranges at 1.1–9.7°C and Δ*t*max 1.0–8.1°C. For the plains, the ranges are smaller with Δ*t*min ranging around 0.7–3.5/0.8–5.7°C and Δ*t*max 0.7–3.4/0.6–5.9°C for RCP 4.5/8.5. Also, for all regions, Δ*t*min is generally higher than Δ*t*max for both RCPs. With minimum temperature projected to rise faster than maximum, future temperature ranges may thus be narrower with higher absolute values than in the past.

Similar consistency in magnitude and direction is not found for annual Δpr over time or space. Δpr has wider spread for plain and hill than the mountain with values

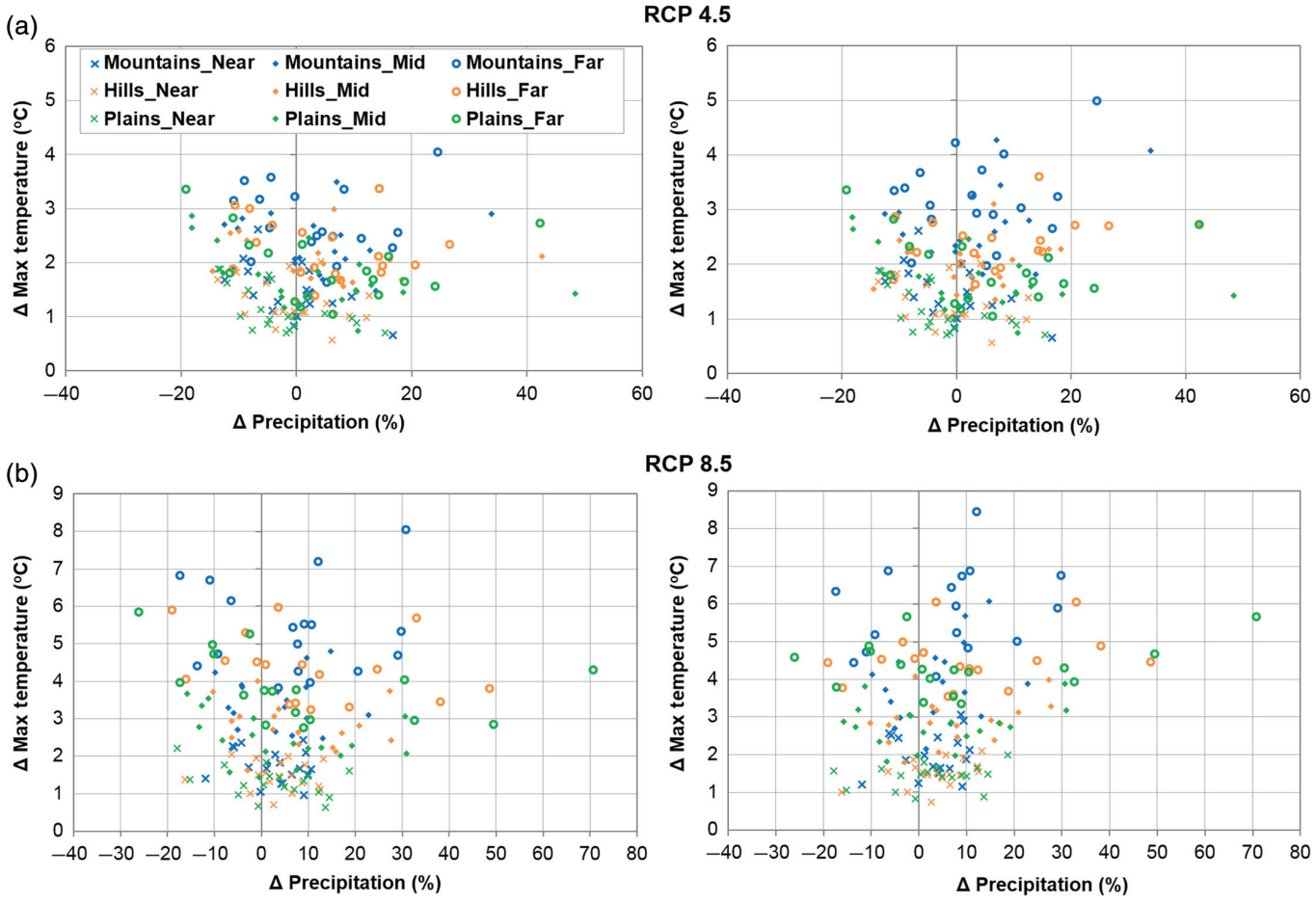

FIGURE 3 Changes in long term 25-year average annual means from historical (1981–2005) to near (2021–2045), mid (2046–2070) and far (2071–2095) future timeframes in RCP 4.5 (top) and RCP 8.5 (bottom) scenarios. Figures on the left show percentage change in long-term average annual total precipitation versus maximum temperature, whereas on the right shows the changes in precipitation versus minimum temperature. Symbol colours distinguish the regions: blue-mountain, orange-hills and green-Tarai plains. Symbol shapes distinguish the timeframes: cross-near, dot-mid and circle-far futures. Refer to web version of the figure for color references [Colour figure can be viewed at wileyonlinelibrary.com]

TABLE 6 Correlation between Δpr, Δ*t*max and Δ*t*min across the three regions for all three timeframes and two RCPs. The colour codes are described in text

		Mountain			Hill			Plain		
For all timeframes for RCP 4.5 and 8.5		**Δpr**	**Δ*t*max**	**Δ*t*min**	**Δpr**	**Δ*t*max**	**Δ*t*min**	**Δpr**	**Δ*t*max**	**Δ*t*min**
Mountain	Δpr	1.00	0.15	0.33	0.80	0.05	0.28	0.75	−0.11	0.22
	Δ*t*max		1.00	0.96	0.24	0.98	0.97	0.25	0.92	0.96
	Δ*t*min			1.00	0.35	0.93	0.97	0.31	0.84	0.95
Hill	Δpr				1.00	0.10	0.33	0.88	−0.06	0.27
	Δ*t*max					1.00	0.95	0.10	0.97	0.96
	Δ*t*min						1.00	0.31	0.89	0.99
Plain	Δpr							1.00	−0.06	0.26
	Δ*t*max								1.00	0.92
	Δ*t*min									1.00

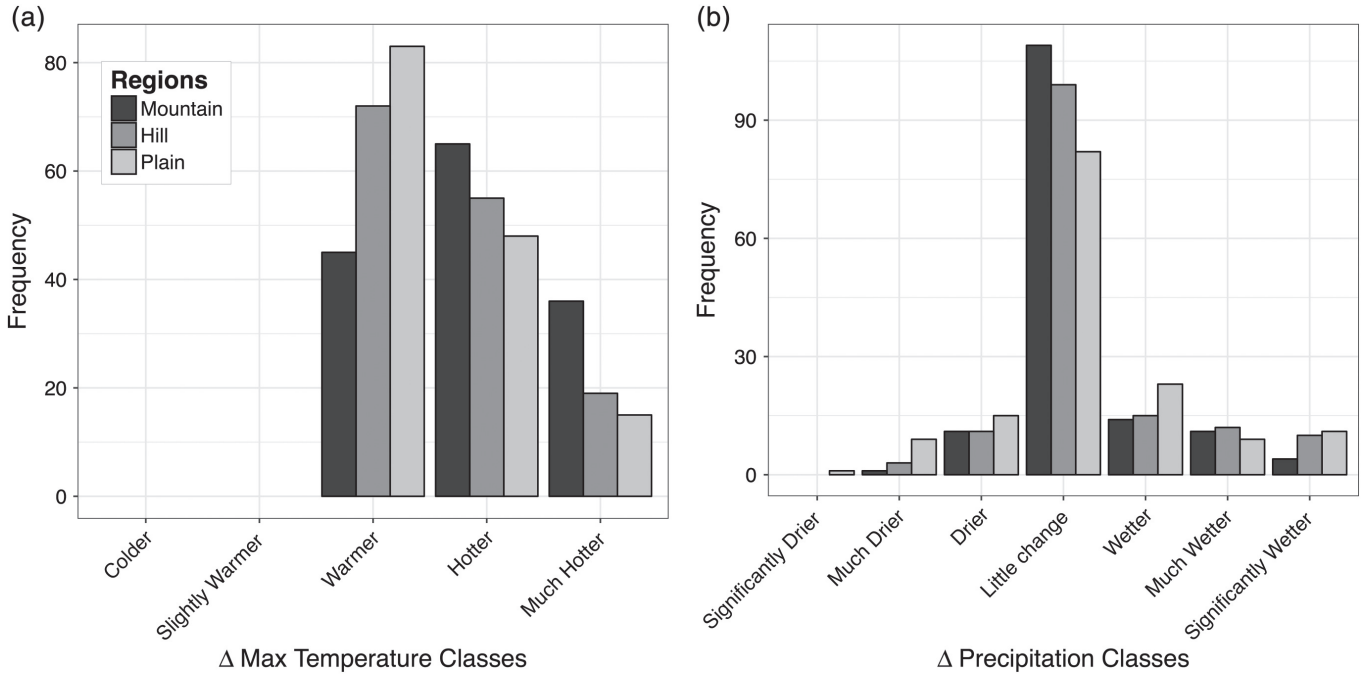

FIGURE 4 Number of models projecting values in each Δ*t*max (left) and Δpr (right) classes defined in Table 4 for the three regions considering model projections under both RCPs for all future timeframes

scattered horizontally. For the plains, Δpr ranges from −19.2 to 48.3% for RCP 4.5 and −26.1 to 70.7% for RCP 8.5, suggesting that the future precipitation is projected to be most erratic in the southern plains. The range for the mountain is narrower at −12.5 to 33.8% for RCP 4.5 and −17.4.1 to 30.8% for RCP 8.5. For hills, the range is similar to the plains for RCP 4.5 from 14.5 to 42.6%. But for RCP 8.5, the Δpr for hills ranges from −19 to 48.6% similar to mountains.

Correlation coefficients (R) listed in Table 6 show strong spatial correlations between the regions. Within each region, there is strong correlation between Δ*t*max and Δ*t*min (highlighted in red with $R = .92–.96$) and Δpr is not correlated to Δ*t*max/min ($R < .33$). Highlighted in blue, the Δpr across plain and hill show higher correlation of $R = .88$ compared to R = .80/.75 between mountain and hill/plain. In future studies, spatial disaggregation between plain and hill may be redundant. Spatial correlations for Δ*t*min (in green) and for Δ*t*max (in orange) are all high ($R > .92$).

3.2 | Climate futures matrices for Western Nepal

Given the high correlation between Δ*t*max and Δ*t*min, only Δ*t*max is considered for setting up the CF matrices. The number of models that fall in each of the Δpr and Δ*t*max

(a)

Plain_RCP8.5_Far	Δ Max temperature				
CF with RCM names	Colder	Slightly Warmer	Warmer	Hotter	Much Hotter
Δ Total precipitation: Significantly Drier					MPI_REMO2009
Much Drier					MPIMR_RegCM4
Drier					MPI_RCA4 CSIRO_RegCM4
Little change				CNRM_CCAM NOAA_RegCM4 CNRM_RCA4	ACCESS_CCAM MPI_CCAM GFDL_CCAM NOAA_RCA4 ICHEC_RCA4
Wetter				CanESM2_RegCM4	
Much Wetter					
Significantly Wetter				MIROC5_RCA4 IPSLLR_RegCM4	HadGEM3-RA IPSLMR_RCA4

(b)

Plain_RCP8.5_Far	Δ Max temperature				
CF with number of RCMs	Colder	Slightly Warmer	Warmer	Hotter	Much Hotter
Δ Total precipitation: Significantly Drier	0	0	0	0	1
Much Drier	0	0	0	0	1
Drier	0	0	0	0	2
Little change	0	0	0	3	5
Wetter	0	0	0	1	0
Much Wetter	0	0	0	0	0
Significantly Wetter	0	0	0	2	2

FIGURE 5 Simple Climate Future Matrix visuals for Tarai plain under the RCP 8.5 far future (2070–2095). (a) Presents name of RCMs in each CF while (b) presents number of models. Orange and Green boxes highlight the representative climate futures for low and high risk cases respectively. See Table 2 for RCM description [Colour figure can be viewed at wileyonlinelibrary.com]

classes are shown in Figure 4. Consistent with global trends, none of the models assessed here for RCP 4.5 and 8.5 project decrease in temperature and very few project dry conditions. For the mountains, model consensus is highest for "Hotter" future while for hills and plains "Warmer" future dominates. Precipitation changes across all three regions predominately fall under the ±10% "Little change" category. The number of models projecting "Little change" is more than three times that of other Δpr classes. Redefining Δpr classes to separate smaller model projections may be considered, keeping in mind that classes should accommodate future RCM additions.

The 18 CF matrices are visualized in three formats provided in Supporting Information S1. Figure 5 present two formats of the matrix for the Tarai plains under RCP 8.5_Far future. Figure 5a shows number of RCMs under each CF while Figure 5b lists the RCM names. Figures 6 and 7 show enhancements where the matrices are shown as classified scatter plots. Colour code indicates model consensus, that is, percentage of the models under each CF cell. Such layering of information helps users visualize the full range of projections and understand where each individual RCMs lie. For a simplified assessment looking at impacts under generic CF, Figure 5 may be sufficient. For a study interested in climate extremes and understanding projection uncertainties, Figures 6 and 7 will be valuable.

Figures 6 and 7 present CF matrices under RCP4.5_Near and RCP8.5_Far scenarios for plain and mountain, respectively. In both regions, the 19 RCMs concentrate around the "Warmer" + "Little Change" cell in RCP 4.5_Near and spread out further for RCP 8.5_Far. Even projection based on the same RCM but driven by different GCMs move in different direction. For example, see points for MPI_RCA4, MIROC5_RCA4 and IPSLMR_RCA4 that belong to the RCA4 RCM family. For both mountain and plain, MPI_RCA4 projections move towards the upper right – "Drier" + "Hotter" corner, while that for MIROC5_RCA4 and IPSLMR_RCA4 move towards the lower right – "Wetter" + "Hotter" corner. The trends for individual RCMs are also not generalizable across the three regions. In Figure 6a,b for the plains, HadGEM_RA projects "Significantly Wetter" conditions but in Figure 7b for the mountains, HadGEM_RA projects "Drier" conditions. This suggests that GCM behaviours dominate RCMs outputs, also noted by Sanjay et al. (2017a).

The matrix-based visualization allows for easy tracking of changes in Δpr and Δ*t*max over the different scenarios for individual RCMs as well as their ensemble behaviour. Such relative progression of RCMs for the across RCPs and futures is shown in the animations in Supporting Information S1. The GIFs show the movement of RCM points for the plains towards higher precipitation changes (both positive and negative) for higher RCPs and futures. For the mountains, the RCM points move more along the temperature axis, where by all RCMs fall under the "Much Hotter" category for RCP 8.5_Far (Figure 7b).

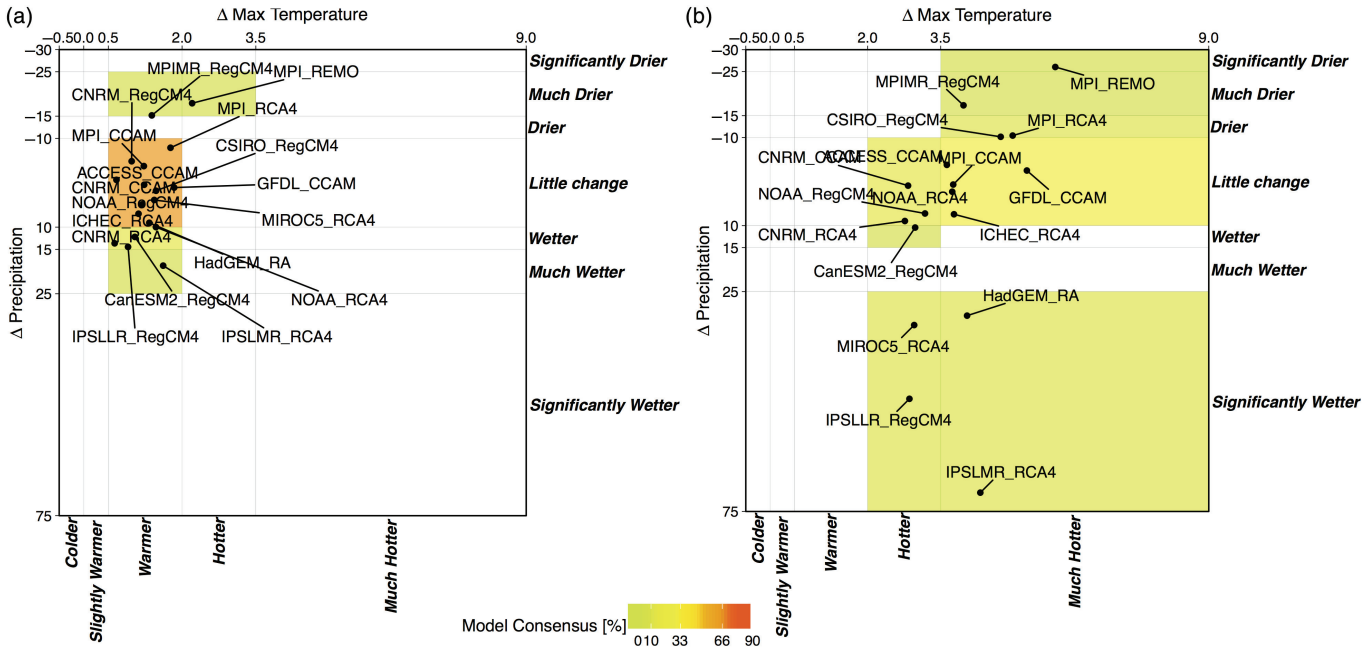

FIGURE 6 Advanced Climate Future Matrix visuals for Tarai plain under (a) RCP 4.5 near future (2021–2045) and (b) RCP 8.5 far future (2070–2095) on the right. See Table 2 for RCM description [Colour figure can be viewed at wileyonlinelibrary.com]

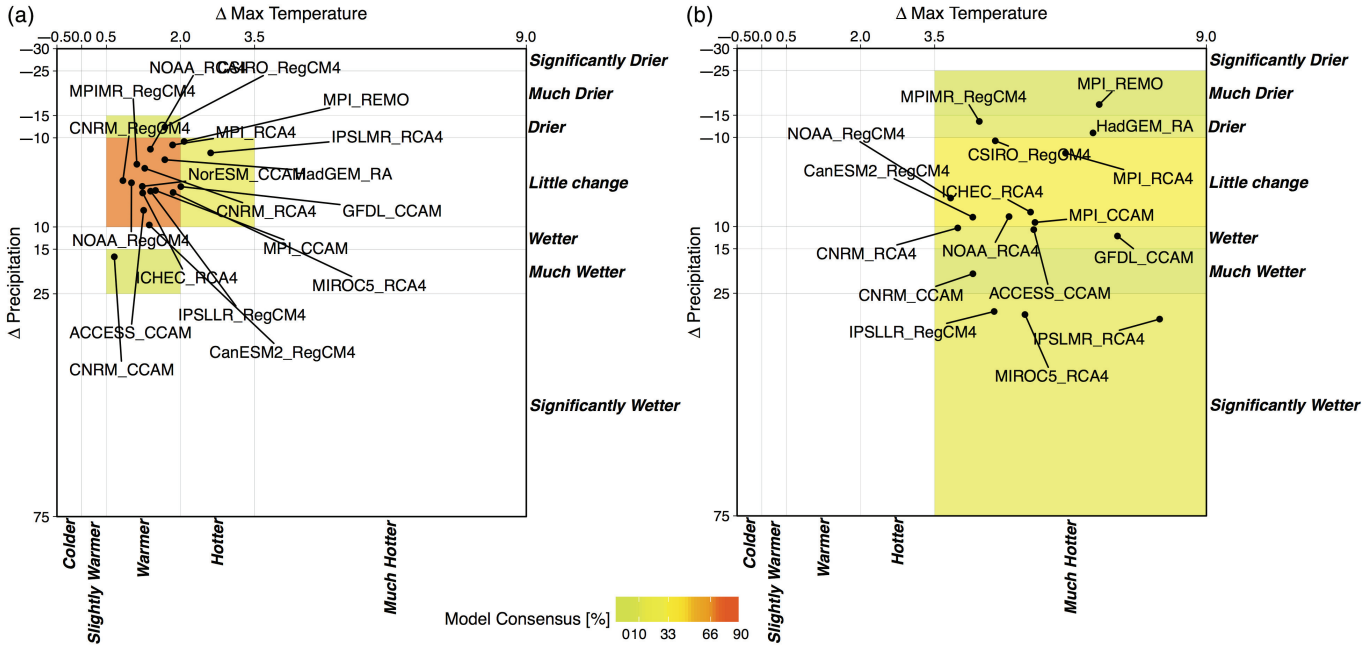

FIGURE 7 Advanced Climate Future Matrix visuals for MOUNTAIN under (a) RCP 4.5 near future (2021–2045) and (b) RCP 8.5 far future (2070–2095) on the right. See Table 2 for RCM description [Colour figure can be viewed at wileyonlinelibrary.com]

3.3 | Application of CF matrices to Karnali

3.3.1 | Selected climate scenarios and relevant RCMs

Table 7 summarize the RCFs and the corresponding RCMs identified from the 18 CF matrices considering long-term water resources management. "Little change" + "Warmer" OR "Hotter" CFs are the dominant RCFs with maximum model consensus across all regions and climate scenarios. The number of models in consensus RCF decreases from 14 RCMs for RCP4.5_Near_Consensus scenario in all three regions to as low as five RCMs for the RCP8.5_Far_Consensus scenarios in hill and plain. Figure 8 shows the RCMs selected across the 18 climate scenarios for each

TABLE 7 Representative climate futures for mountain, hill and terai plain under RCP 4.5 and 8.5 for all three future time frames for application in the Karnali basin water resources assessment study

Case		Near future		Mid future		Far future	
Mountain		**Future**	**# Models**	**Future**	**# Models**	**Future**	**# Models**
RCP 4.5	Low risk	Much Wetter and Warmer	1	Wetter and Warmer	1	Wetter and Warmer	No model
	Consensus	Little change in rain and Warmer	14	Little change in rain and Hotter	9	Little change in rain and Hotter	9
	High risk	Much Drier and Hotter	No model	Much Drier and Hotter	No model	Much Drier and Hotter	No model
RCP 8.5	Low risk	Wetter and Warmer	1	Wetter and Warmer	No model	Wetter and Warmer	No model
	Consensus	Little change in rain and Warmer	10	Little change in rain and Hotter	8	Little change in rain and Much Hotter	7
	High risk	Much Drier and Hotter	No model	Much Drier and Hotter	No model	Much Drier and Much Hotter	1
Hill							
RCP 4.5	Low risk	Wetter and Warmer	2	Much Wetter and Warmer	1	Wetter and Warmer	2
	Consensus	Little change in rain and Warmer	14	Little change in rain and Warmer	10	Little change in rain and Hotter	5
	High risk	Much Drier and Hotter	No model	Much Drier and Hotter	No model	Much Drier and Hotter	No model
RCP 8.5	Low risk	Wetter and Warmer	3	Wetter and Warmer	No model	Wetter and Warmer	No model
	Consensus	Little change in rain and Warmer	12	Little change in rain and Hotter	8	Little change in rain and Much Hotter	6
	High risk	Much Drier and Hotter	No model	Much Drier and Hotter	No model	Much Drier and Much Hotter	2
Plain							
RCP 4.5	Low risk	Wetter and Warmer	1	Wetter and Warmer	5	Wetter and Warmer	3
	Consensus	Little change in rain and Warmer	14	Little change in rain and Warmer	7	Little change in rain and Warmer	5
	High risk	Much Drier and Hotter	No model	Much Drier and Hotter	2	Much Drier and Hotter	1
RCP 8.5	Low risk	Wetter and Warmer	3	Wetter and Warmer	No model	Wetter and Warmer	No model
	Consensus	Little change in rain and Warmer	12	Little change in rain and Hotter	6	Little change in rain and Much Hotter	5
	High risk	Much Drier and Hotter	1	Much Drier and Much Hotter	1	Significantly Drier and Much Hotter	1

region. For cases RCP4.5_Near_Consensus and RCP8.5 _Near_Consensus, nearly all models are selected for all three regions as there is relatively small spread in model values. The MPI_CCAM model is chosen most often across the three regions. IPSLMR_RCA4 is the least chosen – used only once for hills, once for Tarai but never used for mountain. The hits in Table 1 show that, all models are chosen an average of 10 times suggesting that no model is overarching.

Only 10 out of the 18 climate scenarios have representative RCMs available for all three regions. Three scenarios: RCP4.5_Near_High-Risk, RCP8.5_Near_Low-Risk and RCP8.5_Mid_Low-Risk do not have representative RCMs for all regions. Four high-risk scenarios: RCP4.5_Mid_High-Risk, RCP4.5_Far_High-Risk, RCP8.5_Near_High-Risk and RCP8.5_Mid _High-Risk, are only available for the plain. RCP4.5_Far_Low-Risk scenario is not available in the mountains. This suggests that high-risk scenarios are more likely for the plains than in the mountain. However, low-risk scenarios are unlikely across all regions under RCP 8.5. RCP 8.5 is a globally defined scenario representing a case where climate policies are not enforced to limit emissions, leading to high greenhouse gas concentration (Riahi and Grubler, 2007; van Vuuren *et al*., 2011). If climate mitigation efforts are not implemented as assumed by the RCP 8.5 scenario, high-risk futures are virtually certain beyond 2045. Conversely, if stringent climate policies are enforced to lower emissions, as represented by RCP 2.6 not considered in this study, changes in temperature and precipitation are

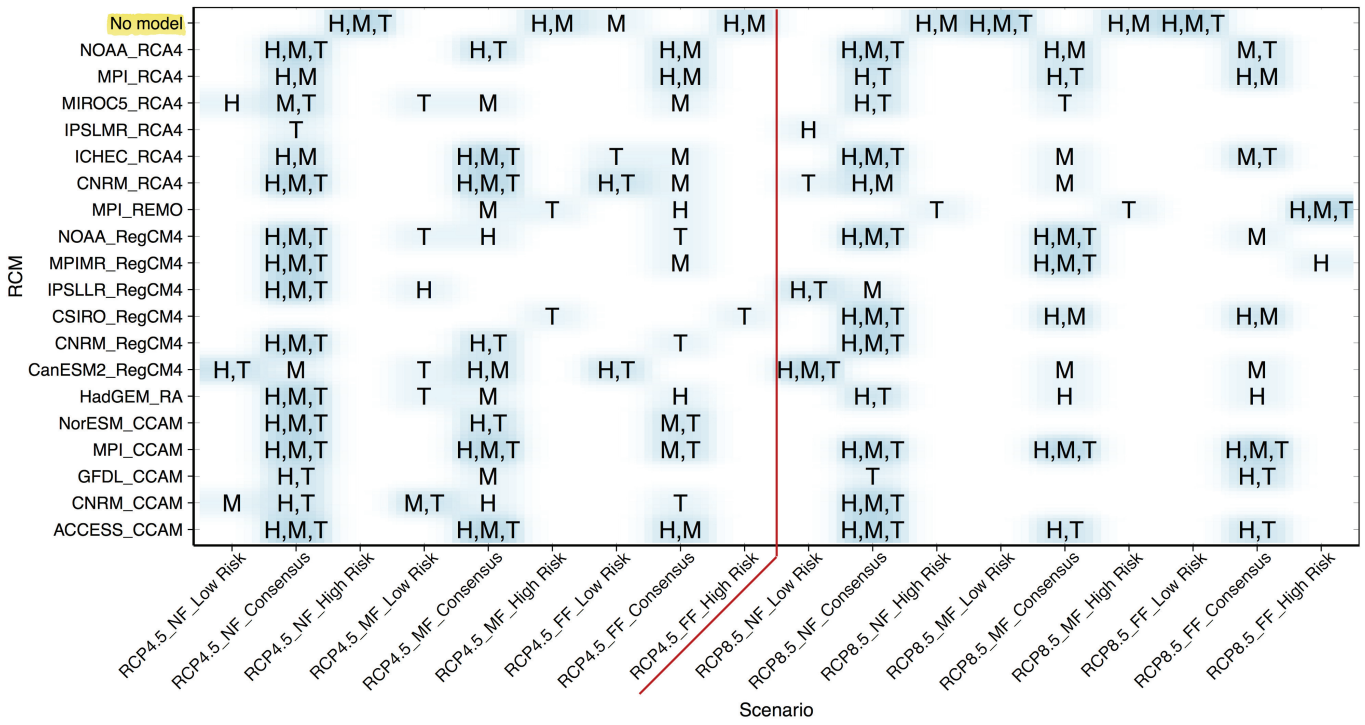

FIGURE 8 RCMs selected for the 18 different climate scenarios for the three regions (M-mountain, H-hill and T-Tarai plain) based on the climate futures matrices in Supporting Information A. See Table 2 for description of the RCMs [Colour figure can be viewed at wileyonlinelibrary.com]

likely to be lower than that presented here for RCP 4.5 and 8.5.

Figure 9 visualizes the role of CF matrices in generating the climate scenarios for Karnali by comparing the ranges in Δpr and Δ*t*max for all available RCMs to that of the ensembles representing the 18 scenarios. The bars show the ensemble means with mean values listed at the top, while the error bars show the ranges across the RCMs. The ranges are narrower for the scenarios than for "all RCMs" as the scenarios selectively group models that agree in projections. The low and high-risk scenarios have even narrower ranges because they comprise of fewer RCMs. Especially for Δpr, it is clear that each climate scenario only samples a portion of the full range of available projections. While Δpr values for all RCMs across all regions and scenarios range from −26.1 to 70.7%, the ensemble means for the scenarios are between −2.8 and 8.9%. The low-risk scenario ensembles across all regions and scenarios have mean Δpr values between 10.5 and 18.2%, consensus between −9.7 and 10.0% and high risk between −26.1 and −16.0%. Similarly, for Δtmax, when considering specifically the far future, Δ*t*max across all regions ranges between 0.9 and 5.9°C for all RCM, 0.6 and 0.2°C for low-risk, 0.6 and6.1°C for consensus and 4.1 and 6.8°C for high-risk cases.

Using an ensemble with all RCMs would in essence only simulate climate scenario with small changes in precipitation as seen for the consensus RCF because climate signals from different RCMs cancel out. Application of CF matrix as an RCM selection criterion prior to ensemble generation allows practitioners to create ensembles that match the climate risk of their interest lending well to a scenario-based impact analysis. The dilution of climate signals when creating ensembles is not as much an issue for Δ*t*max. Nonetheless, analysis that considers RCM selection consciously can provide more robust climate inputs in comparison to random use of RCMs without characterizing the nature of the projections.

3.3.2 | Bias correction of scenario ensembles

Bias-corrected multi-model ensembles were prepared at nine meteorological stations in shown in Figure 1 for the 10 climate scenarios. Stations 202 and 303 lie in the mountain; 104, 406, 513 and 514 in the hill; and 140, 187 and 225 in the plain. Figure 10 presents historical long-term average seasonal total precipitation and maximum temperature based on observed data (black bar), the raw scenario ensembles (dashed lines) and bias-corrected ensembles (coloured bars). The deviation of the raw RCM ensembles from the historical observed values indicate a spatial trend in bias. Consistent with literature listed in Table 5, the raw ensembles show wet biases for mountain stations, both wet and dry biases for hill stations and dry biases for the lower elevation plain stations. Stations 104 (1848 m) and 514 (2,100 m) classified as hilly

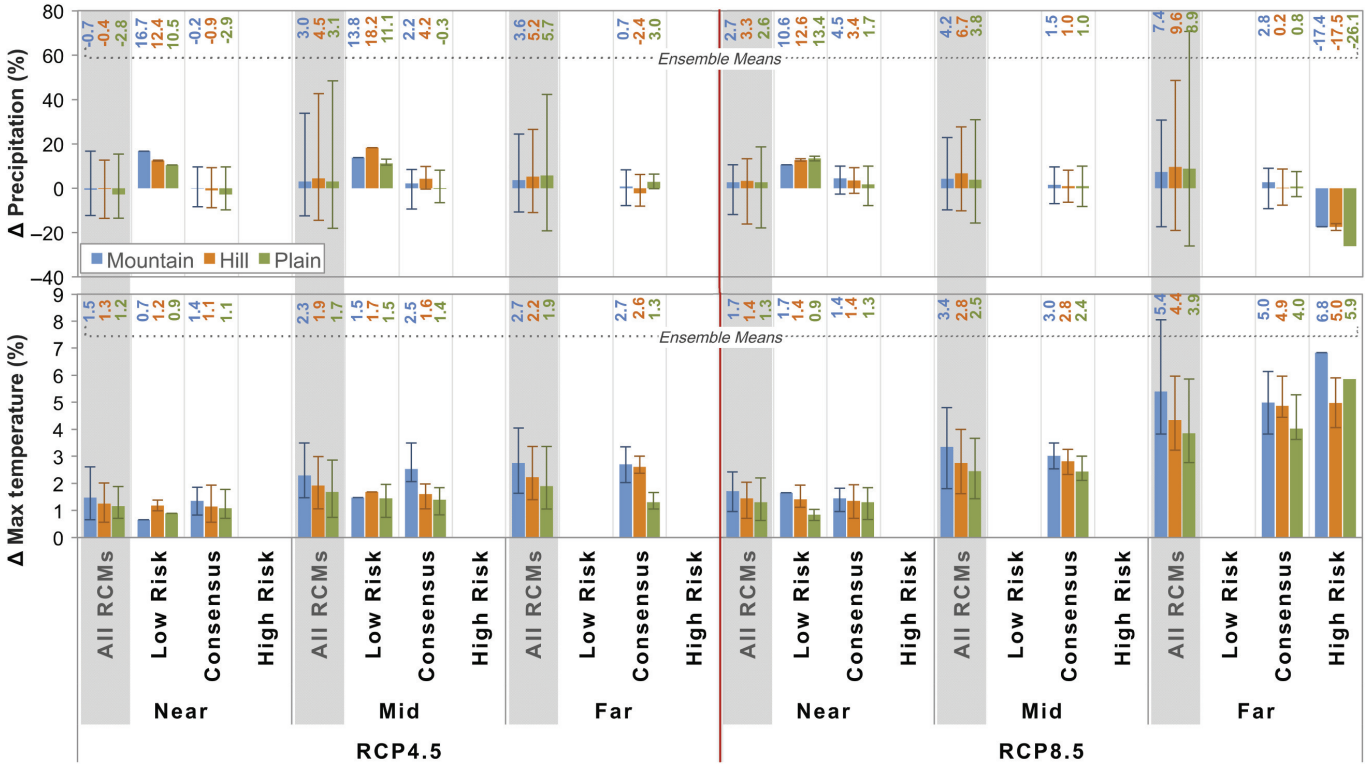

FIGURE 9 Region-wise means (bars) and ranges (error bars) in long-term annual average Δpr and Δ*t*max for all available RCMs (greyed) and representative RCM ensembles for the 18 different climate scenarios combining 2 RCPs (4.5 and 8.5), 3 futures (near, mid, far) and three RCFs (low risk, consensus, high risk). Numbers at the top of graph indicate mean value for each scenario ensemble [Colour figure can be viewed at wileyonlinelibrary.com]

station due to their latitude-longitude lie in relatively high elevations. It is interesting to note that station 104 in particular shows biases expected for the mountain region. Ghimire *et al*. (2015) also find that, RCM precipitation bias varies from −20 to 20% between 0 and6,000 m. Precipitation biases also shows a seasonal trend. In the mountain and hill, there is a wet bias across all seasons for the majority of the scenarios. However, in the plain, there is a dry bias in the monsoon (JJAS) and wet bias in winter (DJF). The least bias is seen for the pre-monsoon (MAM).

In Figure 10b for long-term average seasonal maximum temperature, the raw historical ensemble values lie below the historical observed bar in black across all stations showing systematic cold bias across all seasons and scenarios. Higher biases are seen for the mountain stations than the hill and plain stations. The bias is worst at mountain station 202, with biases as high as −29.5°C in the monsoon (JJAS), while performance is best at hill station 104. The observed cold bias is consistent with Nengker *et al*. (2017)'s findings of seasonal biases of −7°C on average and as high as −14°C for the western HKH. However, these RCM temperature biases are higher compared to GCM biases of −6.0 to 2.5°C reported by Lutz *et al*. (2016) for the entire HKH.

Quantile-mapping performs well, especially for temperature due to the systematic nature of biases. The seasonal performance statistics (NSE, R2 and PBIAS) for raw and bias-corrected RCM ensembles are reported in Supporting Information S3. For precipitation, the NSE for the raw RCM ensembles for the mountain stations are significantly worse (−5.04 to 0.60) than those for the stations in the hill (−0.01 to 0.90) and plain (0.16 to 0.92). Quantile-mapping increases the NSE across all precipitation ensembles to an acceptable range of 0.76 to 0.96 and PBIAS values from (102.8 to 193.4%) to (0.01 to 0.05%). The NSE for maximum temperature is improved from −33.8 to 0.85 for raw ensembles to 0.85 to 0.96 for bias-corrected ensembles, while the PBIAS is improved from 95% to 0% across all stations and scenarios. Meanwhile, the good R2 values for raw historical RCM ensembles for maximum temperature ranging from 0.75 to 0.95 highlight the systematic nature of the temperature bias.

3.3.3 | Future climate projection for Karnali

The solid lines in Figure 10 show seasonal averages for bias-corrected future RCM ensembles for each of the nine meteorological stations. Table 8 lists the range in seasonal and annual averages seen across each region. Future temperatures are higher than historical values across all seasons and stations with highest warming seen in the mountain stations 202 and 303. There is no discernible trend in precipitation.

Figure 11 further explores the seasonal future climate projections presenting the range of projected changes with

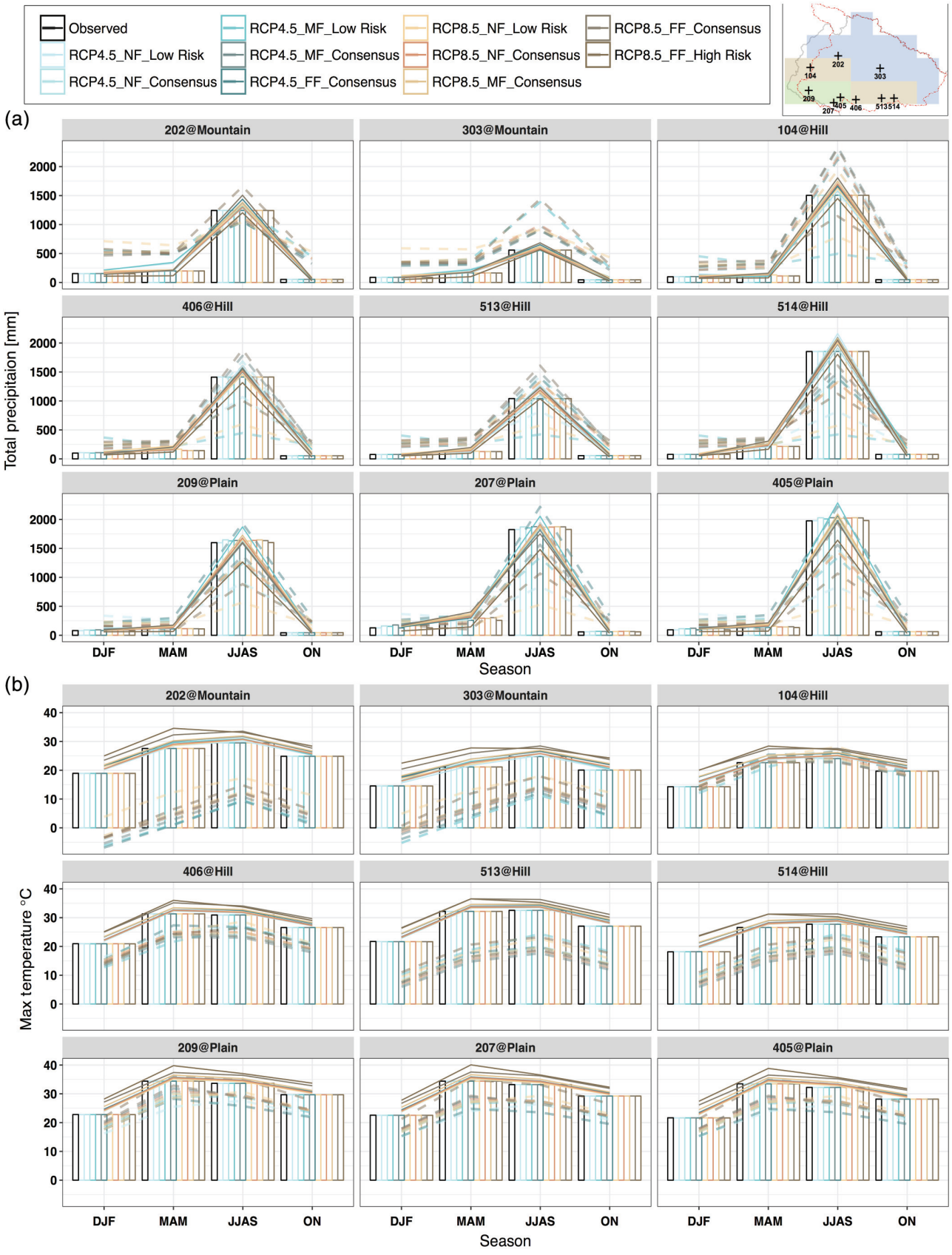

FIGURE 10 Comparison of long-term seasonal averages for (a) total precipitation and (b) maximum temperature in historical and future time frame across the nine meteorological stations. Observed historical station data and bias corrected historical RCM ensembles are shown as bar plots. Raw historical RCM ensembles are shown in dashed lines and bias corrected future RCM ensembles are in solid lines. Colours differentiate the observed (in black), five RCP 4.5 scenarios (in shades of blue) and five RCP 8.5 scenarios (in shades of brown). Refer to web version of the figure for color references. Inset in top right corner shows station locations in Karnali [Colour figure can be viewed at wileyonlinelibrary.com]

respect to the bias-corrected historical values. Δ*t*max is more similar across hills and plains than Δpr. Average Δpr has a wide range in all three regions. However, in Figure 11a the median Δpr across all seasons, scenarios and stations lie close to zero, with whiskers extending in both positive and negative directions. The medians for low-risk scenarios are generally skewed above zero while the single high-risk scenario is negatively skewed. Winter (DJF), pre-monsoon (MAM) and post-monsoon (ON) precipitation projections fluctuate more than monsoon (JJAS), suggested by the higher mean Δpr values and whiskers extending beyond 100% for these seasons. Highest changes are seen in post-monsoon (ON), with averages Δpr as high as 196% projected for the hill and as low as −51.6% in the mountain. While absolute changes in post-monsoon, winter and pre-monsoon precipitation do not appear significant compared to the monsoon in Figure 10a, the high range in percentage changes and low medians in Figure 11a suggest a shift in rainfall pattern. The mean, median and overall distribution of Δpr suggest prolonged monsoon and frequent sporadic rain events even in drier months.

In Figure 11b, Δ*t*max has a clear spatiotemporal trend with higher values and spread seen in the mountain stations, for higher futures and RCPs. All means and medians lie above zero providing strong indication of temperature rise all year-round. Only for the pre-monsoon (MAM) and for mountain stations, some whiskers extend below zero. Average Δ*t*max across all regions is highest for the mountains at 8°C in the winter (DJF) and lowest at 0.4°C in the monsoon (JJAS). The average annual Δ*t*max, ranging 0.5–5.3°C across the mountains and 0.8–4.5°C across the hills and plains are well representative of seasonal changes.

Figure 12 summarizes the changes in average annual Δpr (green) and Δ*t*max (brown/yellow), with red line in each bar chart distinguishing the RCP 4.5 and RCP 8.5 scenarios. Trends in annual Δpr and Δ*t*max across the various scenarios are similar for the stations in the same region. The average annual Δpr ranges from −14.1 to 16.7%, for mountain, −10.3 to 20.7% for hill and −23.8 to 16.4% for plain. Average annual Δpr is negative only for the last bar in each chart for RCP8.5_Far_HighRisk, the only valid high-risk scenario representing dry conditions. Across all regions average seasonal Δpr values (−51.6 to 196.8%) are much higher and variable than annual values (−23.8 to 20.7%). Increasing trends in average annual Δ*t*max across the climate scenarios and stations are similar. Average annual Δ*t*max ranging around 0.5–5.3°C is highest for the mountain, with higher values for RCP 8.5 than RCP 4.5 farther in the future. These spatial variations are consistent with prior observation based on raw RCM data that Δpr appears more prominent in the Tarai while Δ*t*max is more prominent in the mountains.

Presented projections at the nine stations reiterate the spatiotemporal variation in climate even over short distances in heterogeneous terrains. Stations 202 and 303 lie about 120 km apart in the mountains but show difference in seasonal change for both precipitation (Figure 11a) and temperature (Figure 11b). Pattern in station 104 in the hill is similar to that of the mountain stations at similar elevations; though station 514 at higher elevation follows patterns in other hill stations. Scientific advances leading to increase in reliability and resolution of satellite-based climate data and RCMs will be key to ensure future climate assessments can better capture these variations induced by complex topography and microclimates across the over 50,000 km^2 span of Western Nepal.

3.3.4 | Impact assessment study

Figure 12 presents the SWAT simulated percentage changes in average annual discharge ΔQ (blue) at five discharge stations under the 10 climate scenarios. The stations show varying level of sensitivity to change in precipitation and temperature. Specifically, station 215 in the mountain region shows higher increases with ΔQ varying from 48.2 to 63.8% while downstream station like 280 show minimal changes ranging from 01.6 to 11.6%. Maximum decline in discharge is seen in station 220 at −19.1% for the RCP

TABLE 8 Range in seasonal and annual average Δpr and Δ*t*max values across meteorological stations in the three regions. Stations considered within each region are presented in brackets

	DJF	MAM	JJAS	ON	Annual
Mean Δpr (%)					
Mountain (202, 303)	−45.7 to 43.2%	−41.8 to 73.8%	−3.1 to 22.3%	−51.6 to 104%	−14.1 to 16.7%
Hill (104, 406, 513, 514)	−32.5 to 47.7%	−29.7 to 54.5%	−6.9 to 22.9%	−45.7 to 196.8%	−10.3 to 20.7%
Plain (209, 207, 405)	−41.1 to 62.5%	−46.8 to 54.3%	−21 to 14.8%	−46.5 to 123.4%	−23.8 to 16.4%
Mean Δ*t*max (°C)					
Mountain (202, 303)	1.1 to 8.0°C	0.5 to 7.0°C	0.4 to 4.1°C	0.1 to 4.2°C	0.5 to 5.3°C
Hill (104, 406, 513, 514)	0.9 to 5.8°C	1.0 to 5.8°C	0.7 to 3.8°C	0.6 to 4.1°C	0.8 to 4.5°C
Plain (209, 207, 405)	1.1 to 5.8°C	0.6 to 5.7°C	0.6 to 3.4°C	0.5 to 4.0°C	0.8 to 4.5°C

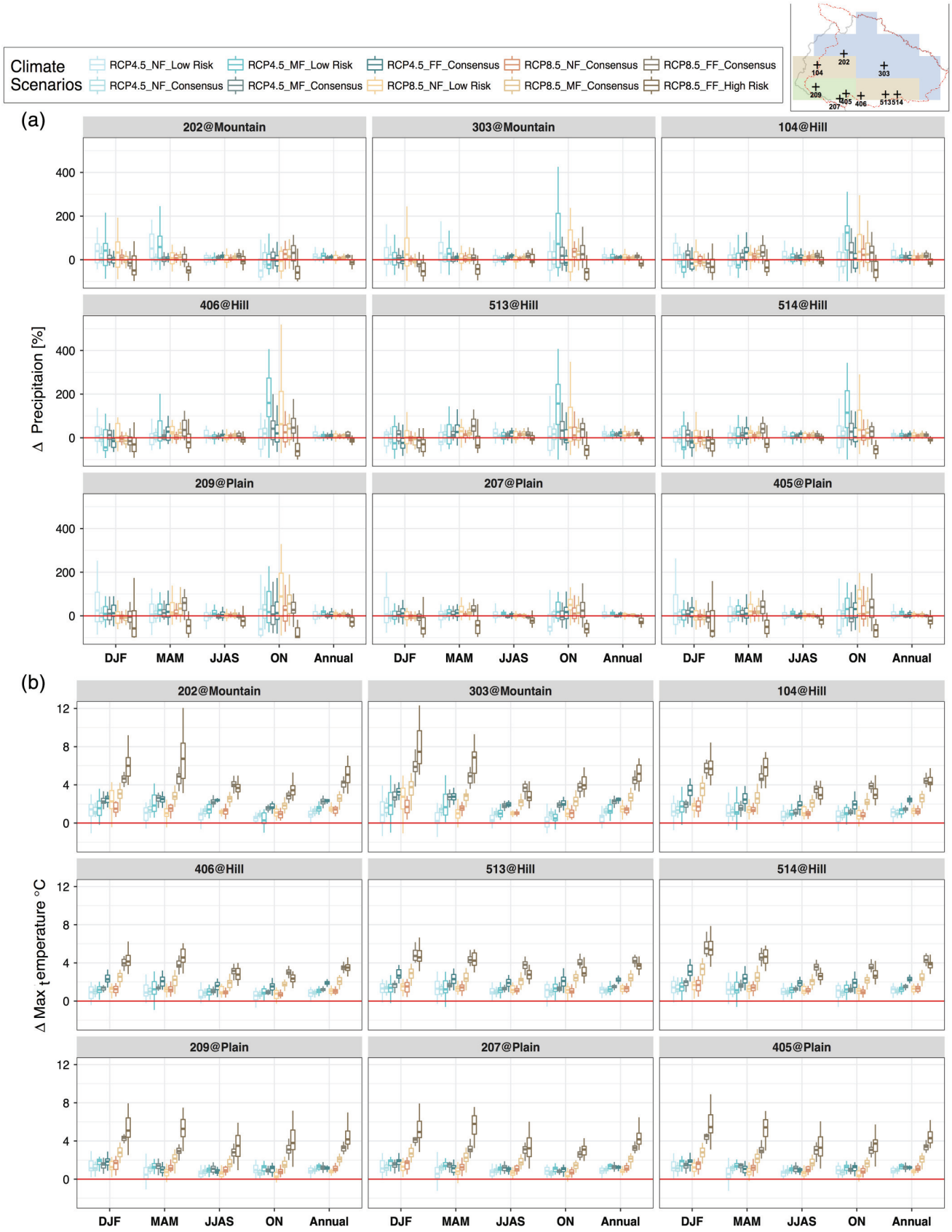

FIGURE 11 Projected changes in of long-term seasonal averages for (a) total precipitation in (%) and (b) maximum temperature in (°C) for the 10 climate scenarios at nine meteorological stations. Change evaluated with respect to historical RCM ensemble corresponding to each climate scenario. See Figure 10 for legend mapping colours to different climate scenarios. Edges of the box plot indicates interquartile range (IQR), interior line indicates median and whiskers indicate lower of ±1.5*IQR or max/min data values. Colours differentiate the five RCP 4.5 scenarios (in shades of blue) and five RCP 8.5 scenarios (in shades of brown). Refer to web version of the figure for color references [Colour figure can be viewed at wileyonlinelibrary.com]

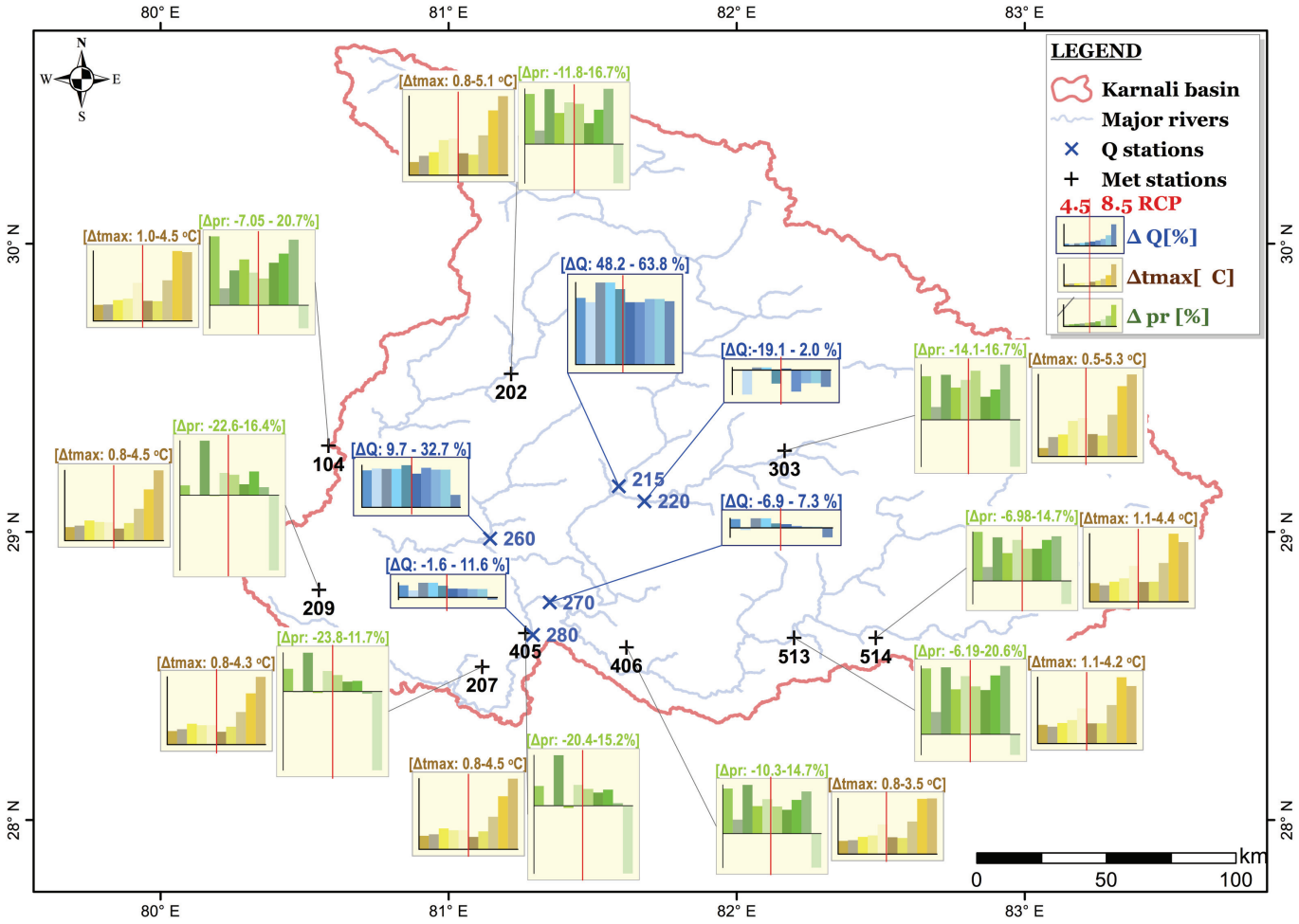

FIGURE 12 Green and brown bar charts show changes in average annual total precipitation (Δpr) and maximum temperature (Δ*t*max) respectively based on bias-corrected multi-RCM ensembles generated for ten climate scenarios at the nine meteorological stations. Blue bar charts show change in annual average discharge (ΔQ) at five discharge stations simulated by the SWAT model for the ten climate scenarios. Value range in each bar chart and unit is indicated above the chart. Order of climate scenarios in bar charts from left to right is: RCP4.5_NF_Low Risk, RCP4.5_NF_Consensus, RCP4.5_MF_Low Risk, RCP4.5_MF_Consensus, RCP4.5_FF_Consensus, RCP8.5_NF_Low Risk, RCP8.5_NF_Consensus, RCP8.5_MF_Consensus, RCP8.5_FF_Consensus, RCP8.5_FF_High Risk [Colour figure can be viewed at wileyonlinelibrary.com]

4.5_NF_Consensus scenario. Stations 220, 270 and 280 appear more resilient to climate change than others at an annual scale. Such difference in response of Q stations to Δpr may relate to location of station along the river. Rising temperatures across the region will increase evapotranspiration, which may explain low ΔQ values in downstream stations given high Δ*t*max for RCP 8.5 scenarios. In RCP8.5_FF_HighRisk, the decline in precipitation across all meteorological stations, simulated decline in discharge only in stations 220, 270 and 280, suggesting that they are rain-fed. The increasing and decreasing trends seen at station 220 and 270 across the different scenarios requires further exploration of the water balance components and upstream-downstream linkages. Such rigorous analysis of sub-annual changes and uncertainties in water balance components is presented in Pandey *et al*. (2018).

3.4 | Uncertainty in the CF framework

The IPCC reports "*low confidence* in projections of many aspects of climate phenomena that influence regional climate change" due to the coarse model resolution and limited scientific understanding of aerosol and cloud processes that are key drivers of climate change (Pg. 115 in Stocker *et al*., 2013). As seen in Figure 10, the bias in precipitation is more complex than temperature bias, potentially due to the complexities of the governing orographic processes of cloud formation. Bias from limitations in existing RCM and GCMs are hard to resolve only by statistical methods (Flato *et al*., 2013; Sanjay *et al*., 2017a). Such model uncertainties become more important at regional and sub-regional scale considered here. Multi-model and multi-scenario analysis using the CF framework is one alternative to consider both

model and scenario uncertainties in climate impact assessments (Knutti *et al*., 2010; Stocker *et al*., 2013).

The CF framework inherently assumes spread in model projections as the only measure of uncertainty and consensus between models as the measure of confidence in the representative climate future. As such, the CF matrix does not provide a measure of total uncertainty. The framework is also sensitive to the models included in the initial ensemble; also, included models may not be independent of each other (Knutti *et al*., 2010). This may exacerbate known biases in CORDEX-SA RCM families and limitations in application of RCMs to finer scales.

The use of raw projections for generating the CF matrices is also contentious. The extent to which past performance of RCMs should be given importance in gauging confidence in future projections is a debate that extends beyond this paper (Wilby, 2010; Flato *et al*., 2013; Whetton *et al*., 2016). Lutz *et al*. (2016) also highlight this difficulty and suggest reordering the steps in their model selection approach to suit user preference. However, the similarity in projection trends in Figure 3 (raw RCMs) and in Figure 11 (bias-corrected RCMs) provides some validation that RCM selection using the raw projection-based CF matrix is reasonable. Nonetheless, raw RCM data should only be used as a first step in grouping RCMs into ensembles. Investigation of past performance and bias correction of selected RCMs to remove models with significantly poor performance is necessary. Further investigation of biases, including impact of CF matrix on biases propagation will be addressed in forthcoming papers.

The spatial scale of application is also debatable. While finer scale is desirable here, working with only a few grids may introduce physical inconsistencies, and inflate RCM uncertainties as explored by Madsen *et al*. (2017). For the case of Western Nepal, the mountain covers majority of the basin while only three grids form the Tarai plains. Combining the hill and plain for future iteration may be desirable. The suitability of using the mountain, hill and plain regions defined by the national Department of Survey as climatic zones also needs to be analysed as projections and biases vary stronger with elevation. In addition, projections discussed here for climate change in Western Nepal may not be generalizable for other parts of the country.

The CF matrices developed here uses annual scale projections. The seasonal analysis of bias-corrected projections plausibly show that the seasonal precipitation signals are not be well reflected by annual averages. Table 5 comparing annual changes reported in literature for the HKH with values obtained for Western Nepal, shows that the spatiotemporal averages can be misleading as decreasing and increasing rainfall signals cancel out providing low values for annual changes. For impact assessments sensitive to climate seasonality, such as flood prediction, extreme analysis etc., CF matrices based on sub-annual changes will be better. Further analysis of seasonal climate change and its impact on different sectors is being conducted and will be presented in the next paper.

3.5 | Climate futures as decision support tools

Though various uncertainties limit the credibility of RCMs, especially at local scales, these represent the best efforts we have. Additionally, changes in the future due to non-physical and anthropogenic activities are hard to capture. The CF framework can be a valuable decision support tool bridging the gap between credibility and usability of climate projection. Many practitioners still prefer traditional single projection measures such as means and median (Whetton *et al*., 2016). Simpler products, like the Climate Futures for Western Nepal presented here, can deliver climate projections and uncertainties in forms that resonate with users, while not requiring them to process large RCM datasets on their own (Whetton *et al*., 2016). The framework provides a middle ground whereby users can still think in terms of single projections while scientists provide some measure of uncertainty visualized in the form of model spread. Better visualization showing how climate change will vary over time under various RCPs is another way to push decision-makers towards measures that minimize such changes. Figures 3, 5–7 visualize essentially the same data with additional layers of information to make decision-makers aware of their model selection process. Additional screening of model can also be done after the CF matrices if desirable (Clarke *et al*., 2011). User-friendly tools like the CF matrices can be a basis for improvement and uptake of RCMs for conducting a robust assessment of climate impacts.

4 | CONCLUSIONS

Using projections of 19 different CORDEX-SA RCMs to develop 18 CF matrices and 10 plausible CF scenarios for long-term water resources planning, this study provides the first comprehensive RCM selection framework for Western Nepal for generating region and application-specific climate projections. We characterize the spatiotemporal variability in future climate across three regions (mountain, hill and plains) of the Karnali basin and evaluate RCM performance for the same. The 10 plausible climate scenarios identified from the 18 CF matrices suggest that high-risk scenarios, with drier and warmer climates, are more likely to occur in the Tarai plains than in the mountain.

For Western Nepal, RCM projections capture spatial variation. The magnitudes of change in climate across the three regions vary, with higher correlation between changes in

hills and plains. Under RCP 4.5 and 8.5, the hill and plain show greater variability in both magnitude and direction of change in rainfall. Increases in temperature are projected across all three regions, with higher Δtmin/max for mountains than hills and Tarai. Projected precipitation shows increasing variability in both directions (wet and dry) further into the future. Comparison of raw projections with that for the greater HKH from literature indicates that values for Western Nepal are generally higher with wider ranges even at annual scale. Spatial disaggregation is thus necessary to identify sub-basin scale change in climate, especially precipitation, for areas like Western Nepal that show high degree of spatial heterogeneity and prevalence of microclimates. Use of coarser national or regional scale averages may underestimate local changes, which are better resolved in RCMs.

Assessment of biases across the nine meteorological stations in Karnali show that precipitation bias varies with elevation, location and season, while temperature bias varies with spatial location. RCM projections consistently show wet bias in the winter across all regions. In the monsoon, there is wet bias in the mountain stations and dry bias in the plain stations. While RCM performances need improvement, it is shown that quantile-mapping performs well for bias correction across all RCMs. The location-sensitive RCM biases highlight the need for location-specific bias correction in heterogeneous terrains. Stations data may thus be more important for bias correction of projections from RCMs than GCMs.

Across Karnali stations, the bias-corrected Δpr project highest values and spread for the post-monsoon season (JJAS), especially in the hills, indicating a potential shift in rainfall pattern with prolonged monsoon and sporadic intense rain events likely even in drier months. Average seasonal Δpr values (−51.6 to 196.8%) are much higher and variable than annual values (−23.8 to 20.7%). The average annual Δtmax, ranging around 0.5–5.3°C across the mountains and 0.8 to 4.5°C across the hills and plains are well representative of seasonal changes. Based on raw and bias-corrected RCM projections for RCP 4.5 and 8.5, it can be concluded that farther in the future, the hills and plains will see most fluctuation in precipitation while the mountains will see highest increases in temperature. Spatial variation in temperature is projected to be narrower, but absolute values for minimum and maximum temperature may increase. The lack of definite direction in precipitation change will be key challenge in management of climate risks.

Evaluation of future water availability in Karnali under the 10 plausible CFs showed that changes in average annual discharge at five discharge stations are not consistent with changes in annual precipitation and temperature. Discharge stations 215, 260 and 280 simulate increasing average annual ΔQ across all scenarios while stations 220 and 270 simulate variable average annual ΔQ ranging from −19.1 to 7.3%. Downstream discharge stations appear more climates resilient with limited changes in ΔQ. Further analysis of water balance components at sub-annual and seasonal scale and its implication is provided in concurrent paper.

A thorough understanding of the spatiotemporal variation in future climate is essential to build climate-resilient ecosystems. It is demonstrated that the CF framework provides a systematic basis to create multi-modal climate scenario ensembles for a robust scenario-based impact assessment by consciously sampling a subsection of all available projections that capture the most relevant climate risks. More importantly, the use of the CF framework for RCM selection can bring about the realization that climate projections should not be considered deterministic. Ideally, the CF will also motivate practitioners to delve deeper, performing additional analysis of uncertainty and biases in projections for a more manageable number of datasets that are directly relevant to their application. As many governments in the global south push for large infrastructure projects and rapid urbanization plans for development similar to the case of Western Nepal, the CF framework can support robust climate change impact assessments to identify climate-resilient development pathways. While an annual scale CF framework is deemed sufficient for long-term water resources management considered in this study, an impact assessment sensitive to seasonal changes should replicate the method to develop monthly or seasonal CF matrices to better capture the seasonal risks and uncertainties.

ACKNOWLEDGEMENTS

This research is supported by: (i) the Sustainable, just and productive water resources development in Western Nepal (DJB) project under the generous support of the American people through the United States Agency for International Development (USAID); and (ii) GRANT: 0358-NEP-Building Climate Resilience of Watersheds in Mountain Eco-regions (BCRWME)—Package 2: Watershed Hydrology Impact Monitoring Research project, between IWMI and the Department of Soil Conservation and Watershed Management, supported by the Asian Development Bank, Nordic Development Fund and Climate Investment Fund. The contents are the responsibility of the authors and do not necessarily reflect the views of USAID or the United States Government. We acknowledge the World Climate Research Programme's Working Group on Regional Climate, and the Working Group on Coupled Modelling, former coordinating body of CORDEX and responsible panel for CMIP5. We also thank the climate modelling groups (listed in Table 1) for producing and making available their model output. We

also acknowledge the Earth System Grid Federation infrastructure an international effort led by the U.S. Department of Energy's Program for Climate Model Diagnosis and Intercomparison, the European Network for Earth System Modelling and other partners in the Global Organization for Earth System Science Portals (GO-ESSP). Lastly, we thank the two anonymous reviews for their comments that helped improve and tighten up the manuscript to its final form.

ORCID

Sanita Dhaubanjar https://orcid.org/0000-0003-2974-0427
Vishnu Prasad Pandey https://orcid.org/0000-0001-5258-7446
Luna Bharati https://orcid.org/0000-0002-6218-3282

REFERENCES

Arnold, J.G., Kiniry, J.R., Srinivasan, R., Williams, J.R., Haney, E.B., and Neitsch, S.L. (2012) *Soil & Water Assessment Tool: Introductory Manual*. College Station, Texas: Texas A&M, AgriLife Research.

Bajracharya, A.R., Bajracharya, S.R., Shrestha, A.B. and Maharjan, S. B. (2018) Climate change impact assessment on the hydrological regime of the Kaligandaki Basin, Nepal. *Science of the Total Environmen*, 625, 837–848. https://doi.org/10.1016/j.scitotenv.2017.12.332.

Bajracharya, S.R., Palash, W., Shrestha, M.S., et al. (2015) Systematic evaluation of satellite-based rainfall products over the Brahmaputra basin for hydrological applications. *Advances in Meteorology*, 2015, 1–17. https://doi.org/10.1155/2015/398687.

Bharati, L., Gurung, P., Jayakody, P., et al. (2014) The projected impact of climate change on water availability and development in the Koshi. *Mountain Research and Development*, 34, 118–130.

Bookhagen, B. and Burbank, D.W. (2010) Toward a complete Himalayan hydrological budget: spatiotemporal distribution of snowmelt and rainfall and their impact on river discharge. *Journal of Geophysical Research - Earth Surface*, 115, 1–25. https://doi.org/10.1029/2009JF001426.

Choudhary, A. and Dimri, A.P. (2018) Assessment of CORDEX-South Asia experiments for monsoonal precipitation over Himalayan region for future climate. *Climate Dynamics*, 50, 3009–3030. https://doi.org/10.1007/s00382-017-3789-4.

Christensen, J.H., Kumar, K.K., Aldrian, E., et al. (2013) Climate phenomena and their relevance for future regional climate change. In: Stocker, T.F., Qin, D., Plattner, G.-K., et al. (Eds.) *Climate Change 2013 the Physical Science Basis: Working Group I Contribution to the Fifth Assessment Report of the Intergovernmental Panel on Climate Change*. Cambridge, United Kingdom and New York, NY: Cambridge University Press, pp. 1217–1308.

Clarke, J.M., Whetton, P.H. and Hennessy, K.J. (2011) Providing application-specific climate projections datasets: CSIRO's climate futures framework. In: *MODSIM2011, 19th International Congress on Modelling and Simulation*. Canberra, Australia: Modelling and Simulation Society of Australia and New Zealand Inc (MSSANZ), pp. 2683–2687. http://www.mssanz.org.au/modsim2011/F5/clarke.pdf.

CSIRO and Bureau of Meteorology, (BOM)(2018) *Module 4: Climate Futures Framework*. Available at: https://www.climatechangeinaustralia.gov.au/en/climate-campus/online-training/climate-futures-framework/ [Accessed 14th May, 2018.

CSIRO and BOM (2015) *Climate Change in Australia: Technical Report*. Australia: CSIRO and Bureau of Meteorology.

Devkota, L.P., Gyawali, R. and Gyawali, D.R. (2015) Impacts of climate change on hydrological regime and water resources management of the Koshi River basin, Nepal. *Journal of Hydrology: Regional Studies*, 4, 502–515. https://doi.org/10.1016/j.ejrh.2015.06.023.

Flato, G., Marotzke, J., Abiodun, B., et al. (2013) Evaluation of climate models. In: Stocker, T.F., Qin, D., Plattner, G.-K., et al. (Eds.) *Climate Change 2013: The Physical Science Basis. Contribution of Working Group I to the Fifth Assessment Report of the Intergovernmental Panel on Climate Change*. Cambridge United Kingdom and New York, NY: Cambridge University Press, pp. 741–866.

Gautam, M.R. and Acharya, K. (2012) Streamflow trends in Nepal. *Hydrological Sciences Journal*, 57, 344–357. https://doi.org/10.1080/02626667.2011.637042.

Ghaju, S. and Alfredsen, K. (2012) Evaluation of satellite based precipitations and their applicability for rainfall runoff modelling in Narayani Basin of Nepal. *Journal of Hydrology and Meteorology*, 8, 22. https://doi.org/10.3126/jhm.v8i1.15569.

Ghimire, S., Choudhary, A. and Dimri, A.P. (2015) Assessment of the performance of CORDEX-South Asia experiments for monsoonal precipitation over the Himalayan region during present climate: part I. *Climate Dynamics*, 50, 2–4. https://doi.org/10.1007/s00382-015-2747-2.

Giorgi, F., Coppola, E., Solmon, F., et al. (2012) RegCM4: model description and preliminary tests over multiple CORDEX domains. *Climate Research*, 52, 7–29. https://doi.org/10.3354/cr01018.

Giorgi, F. and Gutowski, W.J. (2016) Coordinated experiments for projections of regional climate change. *Current Climate Change Reports*, 2, 202–210. https://doi.org/10.1007/s40641-016-0046-6.

Gudmundsson, L., Bremnes, J.B., Haugen, J.E. and Engen-Skaugen, T. (2012) Technical note: downscaling RCM precipitation to the station scale using statistical transformations – a comparison of methods. *Hydrology and Earth System Sciences*, 16, 3383–3390. https://doi.org/10.5194/hess-16-3383-2012.

ICIMOD (2012). *Land Cover of Nepal 2010 [Dataset]*. International Center for Integrated Mountain Development (ICIMOD). Available at: http://rds.icimod.org/Home/DataDetail?metadataId=9224 [Accessed 1st January 2015].

Immerzeel, W.W., van Beek, L.P.H., Konz, M., et al. (2012) Hydrological response to climate change in a glacierized catchment in the Himalayas. *Climatic Change*, 110, 721–736. https://doi.org/10.1007/s10584-011-0143-4.

Ives, J.D., Shrestha, R.B., and Mool, P.K. (2010) *Formation of Glacial Lakes in the Hindu Kush-Himalayas and GLOF Risk Assessment*. Kathmandu: International Centre for Integrated Mountain Development.

IWMI. (2018a) *Hydropower and Irrigation Projects in Western Nepal*. Digo Jal Bikas: International Water Management Institute (IWMI).

IWMI (2018b). *Sustainable, Just and Productive Water Resources Development in Western Nepal (Digo Jal Bikas)*. Available at: http://djb.iwmi.org/ [Accessed 15th May 2018].

Jarvis, A., Reuter, H.I., Nelson, A., and Guevara, E. (2008) Hole-Filled Seamless SRTM Data V4. Available at: http://srtm.csi.cgiar.org [Accessed 20th August 2015].

Karmacharya, J., Shrestha, A., Rajbhandari, R. and Shrestha, M.L. (2007) *Climate Change Scenarios for Nepal Based on Regional Climate Model RegCM3*. Kathmandu: Department of Hydrology and Meteorology, pp. 1–35.

Khatiwada, K., Panthi, J., Shrestha, M. and Nepal, S. (2016) Hydroclimatic variability in the Karnali River basin of Nepal Himalaya. *Climate*, 4, 17. https://doi.org/10.3390/cli4020017.

Knutti, R., Abramowitz, G., Collins, M., Eyring, V., Gleckler, P.J., Hewitson,B., and Mearns, L. (2010) Good practice guidance paper on assessing and combining multi model climate projections. In: Stocker, T.F., Qin, D., Plattner, G.K., Tignor, M., and Midgley, P.M. (Eds.) *Expert Meeting on Assessing and Combining Multi Model Climate Projections*. Bern, Switzerland: IPCC Working Group I Technical Support Unit, University of Bern, p. 15.

Krakauer, N.Y., Pradhanang, S.M., Lakhankar, T. and Jha, A.K. (2013) Evaluating satellite products for precipitation estimation in mountain regions: a case study for Nepal. *Remote Sensing*, 5, 4107–4123. https://doi.org/10.3390/rs5084107.

Kundzewicz, Z.W. and Stakhiv, E.Z. (2010) Are climate models "ready for prime time" in water resources management applications, or is more research needed? *Hydrological Sciences Journal*, 55, 1085–1089. https://doi.org/10.1080/02626667.2010.513211.

Lafon, T., Dadson, S., Buys, G. and Prudhomme, C. (2013) Bias correction of daily precipitation simulated by a regional climate model: a comparison of methods. *International Journal of Climatology*, 33, 1367–1381. https://doi.org/10.1002/joc.3518.

Lutz, A.F., ter Maat, H.W., Biemans, H., et al. (2016) Selecting representative climate models for climate change impact studies: an advanced envelope-based selection approach. *International Journal of Climatology*, 36, 3988–4005. https://doi.org/10.1002/joc.4608.

Mcgregor, J., Veldore V., Thatcher M., Hoffmann P., Katzfey J., Nguyen K. (2013) CCAM simulations for CORDEX South Asia. In: CORDEX Workshop. 28 August 2013. Kathmandu, Nepal: CSIRO Marine and Atmospheric Research.

Madsen, M.S., Langen, P.L., Boberg, F. and Christensen, J.H. (2017) Inflated uncertainty in multimodel-based regional climate projections. *Geophysical Research Letters*, 44, 11,606–11,613. https://doi.org/10.1002/2017GL075627.

McGregor, J.L. and Dix, M.R. (2001) The csiro conformal-cubic atmospheric GCM. *Fluid Mech its Appl*, 61, 197–202. https://doi.org/10.1007/978-94-010-0792-4_25.

Mcsweeney, C., New, M., and Lizcano, G. (2010a). *UNDP Climate Change Country Profiles: Nepal*. New York, NY: United Nations Development Programme. Available at: http://country-profiles.geog.ox.ac.uk [Accessed 13th May 2018].

McSweeney, C., New, M., Lizcano, G. and Lu, X. (2010b) The UNDP climate change country profiles improving the accessibility of observed and projected climate information for studies of climate change in developing countries. *Bulletin of the American Meteorological Society*, 91, 157–166. https://doi.org/10.1175/2009BAMS2826.1.

McSweeney, C.F., Jones, R.G. and Booth, B.B.B. (2012) Selecting ensemble members to provide regional climate change information. *Journal of Climate*, 25, 7100–7121. https://doi.org/10.1175/JCLI-D-11-00526.1.

Mishra, Y., Nakamura, T., Babel, M.S., et al. (2018) Impact of climate change on water resources of the Bheri River basin, Nepal. *Water*, 10, 220. https://doi.org/10.3390/w10020220.

Moufouma-Okia, W. and Jones, R. (2014) Resolution dependence in simulating the African hydroclimate with the HadGEM3-RA regional climate model. *Climate Dynamics*, 44, 609–632. https://doi.org/10.1007/s00382-014-2322-2.

Mukherjee, S., Hazra, A., Kumar, K., Nandi, S.K. and Dhyani, P.P. (2017) Simulated projection of ISMR over Indian Himalayan region: assessment from CSIRO-CORDEX South Asia experiments. *Meteorology and Atmospheric Physics*, 131, 1–17. https://doi.org/10.1007/s00703-017-0547-4.

Müller, M.F. and Thompson, S.E. (2013) Bias adjustment of satellite rainfall data through stochastic modeling: methods development and application to Nepal. *Advances in Water Resources*, 60, 121–134. https://doi.org/10.1016/j.advwatres.2013.08.004.

Nengker, T., Choudhary, A. and Dimri, A.P. (2017) Assessment of the performance of CORDEX-SA experiments in simulating seasonal mean temperature over the Himalayan region for the present climate: part I. *Climate Dynamics*, 0, 1–31. https://doi.org/10.1007/s00382-017-3597-x.

Palazzi, E., von Hardenberg, J. and Provenzale, A. (2013) Precipitation in the Hindu-Kush Karakoram Himalaya: observations and future scenarios. *Journal of Geophysical Research – Atmospheres*, 118, 85–100. https://doi.org/10.1029/2012JD018697.

Pandey VP, Dhaubanjar S, Bharati L, Thapa BR (2018) *Climate Change Impacts on Spatio-Temporal Distribution of Water Availability in Karnali-Mohana Basin*. Manuscript Under Submission.

Pandey, V.P., Dhaubanjar, S., Bharati, L. and Thapa, B.R. (2019) Hydrological response of Chamelia watershed in Mahakali Basin to climate change. *Science of the Total Environment*, 650, 365–383. https://doi.org/10.1016/J.SCITOTENV.2018.09.053.

Peña-Arancibia, J.L., van Dijk, A.I.J.M., Renzullo, L.J. and Mulligan, M. (2013) Evaluation of precipitation estimation accuracy in reanalyses, satellite products, and an ensemble method for regions in Australia and south and East Asia. *Journal of Hydrometeorology*, 14, 1323–1333. https://doi.org/10.1175/JHM-D-12-0132.1.

Riahi, K., Grübler, A., and Nakicenovic, N. (2007) *Scenarios of Long-Term Socio-Economic and Environmental Development under Climate Stabilization*. Technol Forecast Soc Change, 74, 887–935. https://doi.org/10.1016/j.techfore.2006.05.026

Rummukainen, M., Rockel, B., Bärring, L., et al. (2015) Twenty-first-century challenges in regional climate modeling. In: *Bulletin of the American Meteorological Society*. Boston, MA: American Meteorological Society, pp. 135–138.

Samuelsson, P., Jones, C.G., Willén, U., et al. (2011) The Rossby Centre regional climate model RCA3: model description and performance. *Tellus: Series A, Dynamic Meteorology and Oceanography*, 63, 4–23. https://doi.org/10.1111/j.1600-0870.2010.00478.x.

Sanjay, J., Krishnan, R., Shrestha, A.B., et al. (2017a) Downscaled climate change projections for the Hindu Kush Himalayan region using CORDEX South Asia regional climate models. *Advances in Climate Change Research*, 8, 185–198. https://doi.org/10.1016/j.accre.2017.08.003.

Sanjay, J., Ramarao, M.V.S., Mujumdar, M. and Krishnan, R. (2017b, 2017) Regional climate change scenarios. In: Rajeevan, M.N. and Nayak, S. (Eds.) *Observed Climate Variability and Change over*

the Indian Region. Singapore: Springer G. Springer Science+Business Media, pp. 285–305.

Sharma, R.H. and Awal, R. (2013) Hydropower development in Nepal. *Renewable and Sustainable Energy Reviews*, 21, 684–693. https://doi.org/10.1016/j.rser.2013.01.013.

Shiwakoti, S. (2017) *Hydrological Modeling and Climate Change Impact Assessment Using HBV Light Model: A Case Study of Karnali River Basin*. In: XVI World Water Congress, Cancun, Mexico. Paris, France: International Water Resources Association (IWRA), pp 1–19. Page

Shrestha, H., Bhattarai, U., Dulal, K.N., Adhikari, S., Marahatta, S., and Devkota, L.P. (2015) Impact of climate change on precipitation in the Karnali basin. In: Shrestha, D., Regmi, S.K., Kayastha, R.B. (Eds.) *National Symposium on Hydrology and Meteorology. Nepal, Kathmandu*, p A-7.

Shrestha, S., Khatiwada, M., Babel, M.S. and Parajuli, K. (2014) Impact of climate change on river flow and hydropower production in Kulekhani hydropower project of Nepal. *Environmental Processes*, 1, 231–250. https://doi.org/10.1007/s40710-014-0020-z.

Siddiqui, S., Bharati, L., Pant, M., Gurung, P., Rakhal, B. and Maharjan, D.L. (2012) *Climate Change and Vulnerability Mapping in Watersheds in Middle and High Mountains of Nepal*. Colombo, Sri Lanka: International Water Management Institute (IWMI).

Stocker, T.F., Qin, D., Plattner, G.K., Alexander,L.V., Allen, S.K., Bindoff, N.L., Bréon,F.M., Church, J.A., Cubasch, U., Emori, S., Forster, P., Friedlingstein, P., Gillett,N., Gregory, J.M., Hartmann, D.L., Jansen, E., Kirtman, B., Knutti, R., KrishnaKumar, K., Lemke, P., Marotzke, J., Masson-Delmotte, V., Meehl, G.A., Mokhov, I.I.,Piao, S., Ramaswamy, V., Randall, D., Rhein, M., Rojas, M., Sabine, C., Shindell,D., Talley, L.D., Vaughan D.G., and Xie, S.P. (2013) Technical summary. In: Stocker, T.F., Qin, D., Plattner, G.-K., Tignor, M., Allen, S.K., Boschung, J., Nauels, A., Xia, Y., Bex, V. and Midgley, P.M. (Eds.) *Climate Change 2013: The Physical Science Basis. Contribution of Working Group I to the Fifth Assessment Report of the Intergovernmental Panel on Climate Change. Cambridge: Cambridge University Press*, pp. 33–115.

Thevakaran, A., McGregor, J. L., Katzfey, J., Hoffmann, P., Suppiah, R., & Sonnadara, D. U. J. (2015) An assessment of CSIRO Conformal Cubic Atmospheric Model simulations over Sri Lanka. *Climate Dynamics*, 46(5–6), 1861–1875. https://doi.org/10.1007/s00382-015-2680-4.

Teichmann, C., Eggert, B., Elizalde, A., et al. (2013) How does a regional climate model modify the projected climate change signal of the driving GCM: a study over different CORDEX regions using REMO. *Atmosphere (Basel)*, 4, 214–236. https://doi.org/10.3390/atmos4020214.

Teutschbein, C. and Seibert, J. (2012) Bias correction of regional climate model simulations for hydrological climate-change impact studies: review and evaluation of different methods. *Journal of Hydrology*, 457, 12–29. https://doi.org/10.1016/j.jhydrol.2012.05.052.

Themeßl, M.J., Gobiet, A. and Heinrich, G. (2012) Empirical-statistical downscaling and error correction of regional climate models and its impact on the climate change signal. *Climatic Change*, 112, 449–468. https://doi.org/10.1007/s10584-011-0224-4.

Thiemig, V., Rojas, R., Zambrano-Bigiarini, M. and De Roo, A. (2013) Hydrological evaluation of satellite-based rainfall estimates over the Volta and Baro-Akobo Basin. *Journal of Hydrology*, 499, 324–338. https://doi.org/10.1016/j.jhydrol.2013.07.012.

van Vuuren, D.P., Edmonds, J., Kainuma, M., et al. (2011) The representative concentration pathways: an overview. *Climatic Change*, 109, 5–31. https://doi.org/10.1007/s10584-011-0148-z.

Weaver, C.P., Lempert, R.J., Brown, C., et al. (2013) Improving the contribution of climate model information to decision making: the value and demands of robust decision frameworks. *Wiley Interdisciplinary Reviews: Climate Change*, 4, 39–60. https://doi.org/10.1002/wcc.202.

Whetton, P., Hennessy, K., Clarke, J., et al. (2012) Use of representative climate futures in impact and adaptation assessment. *Climatic Change*, 115, 433–442. https://doi.org/10.1007/s10584-012-0471-z.

Whetton, P.H., Grose, M.R. and Hennessy, K.J. (2016) A short history of the future: Australian climate projections 1987–2015. *Clim. Serv.*, 2–3, 1–14.

Wilby, R.L. (2010) Evaluating climate model outputs for hydrological applications. *Hydrological Sciences Journal*, 55, 1090–1093. https://doi.org/10.1080/02626667.2010.513212.

SUPPORTING INFORMATION

Additional supporting information may be found online in the Supporting Information section at the end of this article.

How to cite this article: Dhaubanjar S, Prasad Pandey V, Bharati L. Climate futures for Western Nepal based on regional climate models in the CORDEX-SA. *Int J Climatol*. 2019;1–25. https://doi.org/10.1002/joc.6327